JOURNAL OF GEOPHYSICAL RESEARCH, VOL. 108, NO. D12, 4353, doi:10.1029/2002JD002890, 2003

Moment-based simulation of microphysical properties of sulfate aerosols in the eastern United States: Model description, evaluation, and regional analysis

Shaocai Yu,[1] Prasad S. Kasibhatla, and Douglas L. Wright
Nicholas School of the Environmental and Earth Sciences, Duke University, Durham, North Carolina, USA

Stephen E. Schwartz and Robert McGraw
Atmospheric Sciences Division, Brookhaven National Laboratory, Upton, New York, USA

Aijun Deng
Department of Meteorology, Pennsylvania State University, University Park, Pennsylvania, USA

Received 28 August 2002; revised 9 December 2002; accepted 19 February 2003; published 19 June 2003.

[1] A six-moment microphysics module for sulfate aerosols based on the quadrature method of moments has been incorporated in a host 3-D regional model, the Multiscale Air Quality Simulation Platform. Model performance was examined and evaluated by comparison with in situ observations over the eastern United States for a 40-day period from 19 July to 28 August 1995. The model generally reproduces the spatial patterns (sulfate mixing ratios and wet deposition) over the eastern United States and time series variations of sulfate mass concentrations. The model successfully captured the observed size distribution in the accumulation mode (radius 0.1–0.5 μm), in which the sulfate is predominately located, while underestimating the nucleation and coarse modes on the basis of the size distributions retrieved from the modeled six moments at the Great Smoky Mountains (GSM). This is consistent with better model performance on the effective radius (ratio of third to second moment, important for light scattering) than on number-mean and mass-mean radii. However, the model did not predict some of the moments well, especially the higher moments and during the dust events. Aerosol components other than sulfate such as dust and organics appear to have contributed substantially to the observed aerosol loading at GSM. The model underpredicted sulfate mixing ratios by 13% with about 50% of observations simulated to within a factor of 2. One of the reasons for this underestimation may be overprediction of sulfate wet deposition. Sulfate mass concentrations and number concentrations were high in the source-rich Ohio River valley, but number concentrations were also high over the mid-Atlantic coast (New Jersey area). Most (77%) sulfate amount was below 2.6 km, whereas most sulfate number (>52%) was above 2.6 km except over Ohio River valley (41%). These results demonstrate the accuracy, utility, practicality, and efficiency of moment-based methods for representing aerosol microphysical processes in large-scale chemical transport models. *INDEX TERMS:* 0305 Atmospheric Composition and Structure: Aerosols and particles (0345, 4801); 0345 Atmospheric Composition and Structure: Pollution—urban and regional (0305); 0365 Atmospheric Composition and Structure: Troposphere—composition and chemistry; 0368 Atmospheric Composition and Structure: Troposphere—constituent transport and chemistry; *KEYWORDS:* moment-method, sulfate aerosol, model simulation, microphysical properties, eastern United States

Citation: Yu, S. C., P. S. Kasibhatla, D. L. Wright, S. E. Schwartz, R. McGraw, and A. Deng, Moment-based simulation of microphysical properties of sulfate aerosols in the eastern United States: Model description, evaluation, and regional analysis, *J. Geophys. Res.*, *108*(D12), 4353, doi:10.1029/2002JD002890, 2003.

1. Introduction

[2] The sulfur cycle over North America has been simulated with regional and global 3-D chemical transport models (CTMs) by many investigators [*Langner and Rodhe*, 1991; *Kasibhatla et al.*, 1997a; *Benkovitz and Schwartz*, 1997; *Chin et al.*, 2000; *Von Salzen et al.*,

[1]Now at Atmospheric Sciences Modeling Division, National Exposure Research Laboratory, U.S. Environmental Protection Agency, Research Triangle Park, North Carolina, USA.

0148-0227/03/2002JD002890$09.00

2000; *Rasch et al.*, 2000]. Most of these models have simulated only the mass concentration of sulfate aerosol and not size distributions. However, representing the microphysical properties of aerosols (i.e., their intensive properties [*Ogren*, 1995]) in addition to their mass concentrations (extensive properties) and understanding the influence of aerosol microphysical processes on properties of tropospheric aerosols are important because environmental effects of aerosols such as atmospheric visibility, climate change, acid deposition, and health effects depend not just on the mass concentration but also on the size distribution and chemical composition of these particles [*Sisler and Malm*, 2000; *Yu et al.*, 2000, 2001; *Schwartz*, 1996; *Penner et al.*, 2002; *Ghan et al.*, 2001]. Additionally, the mass loading of aerosols is itself influenced by processes whose rates depend on particle size. It is therefore necessary to include a microphysical representation of aerosol formation, evolution, and removal processes in atmospheric CTMs. Most previous approaches to aerosol microphysical modeling have simulated the particle distribution function (PDF) either explicitly, by a bin-sectional approach [*Whitby and McMurry*, 1997; *Russell and Seinfeld*, 1998; *Von Salzen et al.*, 2000; *Jacobson*, 2002] or by a multimodal approach [*Whitby and McMurry*, 1997; *Binkowski and Shankar*, 1995; *Wilson et al.*, 2001], in which particle size distributions are represented as the superposition of three lognormal subdistributions, or modes.

[3] Recently, an alternative approach has been introduced that represents the aerosol in terms of the moments of the PDF [*McGraw*, 1997; *Barrett and Webb*, 1998]. The radial moments are defined as $\mu_k = \int_0^\infty r^k f(r) dr$, where μ_k is the kth radial moment, r is radius, and $f(r)$ is the PDF for the number size distribution. The advantages of the method of moments (MOM) include comparatively straightforward implementation of the method as the moments evolve according to sets of differential equations having the same structure as the rate equations describing the evolution of reacting chemical species in the same background flow and freedom from errors associated with numerical diffusion in particle-size space [*McGraw*, 1997]. Another advantage of the MOM is the small number of variables required to represent aerosol properties; the six lowest-order radial moments directly give important aerosol properties: particle number concentration (μ_0), particle mass concentration ($4\pi\rho\mu_3/3$; ρ is particle density), number mean radius ($r_n = \mu_1/\mu_0$), effective radius ($r_e = \mu_3/\mu_2$), mass mean radius ($r_m = \mu_4/\mu_3$), and the standard deviation ($\sigma = [\mu_0\mu_2 - \mu_1^2]^{1/2}/\mu_0^2$) characterizing the width of the PDF [*McGraw*, 1997; *Wright et al.*, 2000]. The more recently introduced quadrature method of moments (QMOM) [*McGraw*, 1997] overcomes closure difficulties inherent in the MOM, and allows condensation and coagulation kernels of arbitrary functional form to be treated without a priori assumptions regarding the form of the PDF. The utility of the MOM has been further enhanced by the development of methods such as Randomized Minimization Search Technique (RMST) and Multiple Isomomental Distribution Aerosol Surrogate (MIDAS), which use the first six moments to compute aerosol optical properties to within 1–2% of those obtained directly from the PDF [*Yue et al.*, 1997; *Wright*, 2000; *Wright et al.*, 2002]. Even properties requiring integration over only a portion of the full size spectrum of the PDF, such as cloud activation, or properties relevant to the PM 2.5/10 standards can be computed to an accuracy of about 10% or better [*Wright et al.*, 2002].

[4] Building on these developments in the MOM approach, we implement a six-moment aerosol microphysical module 6M [*Wright et al.*, 2001] in a regional atmospheric CTM, and use this newly developed capability to simulate the summertime distribution of sulfate aerosols over the eastern United States. Our focus on sulfate aerosols stems from studies which show that this is the dominant anthropogenic aerosol component in the eastern United States [e.g., *Sisler and Malm*, 2000]. We present a detailed evaluation of model performance by comparing simulated particle mass and number concentrations, size parameters (effective radius, mass mean radius, and number mean radius), and surrogates to the underlying size distributions with observations.

[5] This work may be most closely compared to that of *Von Salzen et al.* [2000], who simulated the responses of sulfate aerosol size distributions over North America to SO_x emissions and H_2O_2 concentrations for 1994 summer and winter. Our study is distinguished from that of *Von Salzen et al.* [2000] in three important aspects: (1) the use of QMOM to simultaneously track the six lowest-order radial moments of a particle size distribution; (2) the evaluation of model performance against regional spatial and temporal variations of in situ measurements for aerosol mass and number concentrations, and size parameters over eastern United States; and (3) an analysis of regional budget of sulfate mass and number concentrations over the eastern United States.

2. Model Description

[6] The host 3-D regional CTM is the nonhydrostatic version of the Multiscale Air Quality Simulation Platform (MAQSIP) [*Odman and Ingram*, 1996]. MAQSIP is a prototype of US Environmental Protection Agency (EPA) Models-3 Community Multiscale Air Quality (CMAQ) Modeling System [*Byun and Ching*, 1999]. The model domain covers the eastern United States with a horizontal grid of 72 × 74 36-km grid cells (see Figure 1). The vertical resolution is 22 layers, which are set on a sigma coordinate, from the surface to ~160 hPa. The model was driven by meteorological fields from the MM5 meteorological model [*Grell et al.*, 1994]. The prognostic variables in the model are the gas phase concentrations of SO_2 and H_2SO_4, and the first six radial aerosol moments. In the following sections, we describe the various components of the model as configured for this study.

2.1. Aerosol Dynamics and Microphysics

[7] Aerosol microphysical processes are simulated using the module 6M [*Wright et al.*, 2001] which is based upon the QMOM [*McGraw*, 1997] and MIDAS [*Wright*, 2000] techniques. The QMOM represents integrals over a size distribution using a set of abscissas and weights derived from the lower-order moments and requires no assumption about the distribution other than that it has well-defined moments. There are special cases where we assumed that the aerosol size distribution is lognormal. These are (1) for primary emissions and (2) for use with the cloud activation

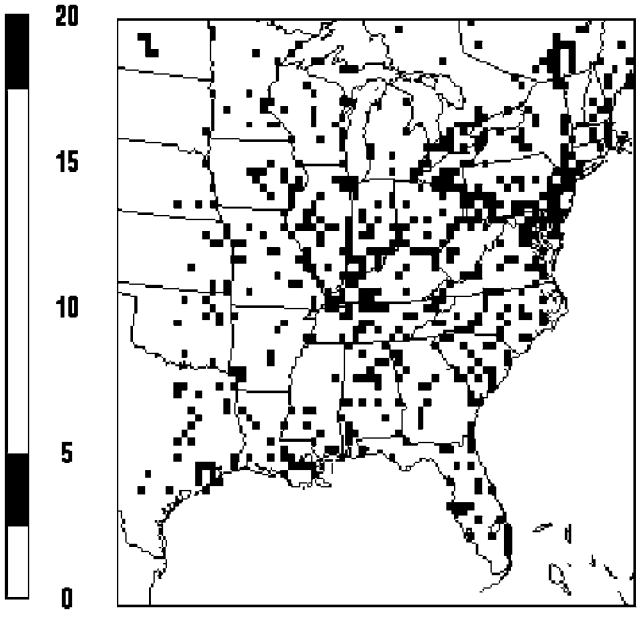

Figure 1. The MAQSIP model domain and distribution of sulfur (SO_2 + SO_4^{2-}) emission over the eastern United States in summer, including both surface and elevated sources (see text). Unit is g m^{-2} yr^{-1}. See color version of this figure at back of this issue.

parameterization of *Abdul-Razzak et al.* [1998]. However, the reasons for assuming a lognormal in these cases are not inherently related to the QMOM. Indeed, we evolve six moments via the three-point QMOM. For parameterization of a single lognormal distribution only three would have been required. By comparison with results obtained using a high-resolution discrete model of the particle dynamics, *Wright et al.* [2001] show that the accuracy of 6M is good relative to uncertainties associated with other processes represented in atmospheric CTMs. Differences between 6M and the discrete model in the mass/volume moments and in the partitioning of sulfur (VI) between the gas and aerosol phases remain under 1% whenever significant aerosol is present, and differences in particle number rarely exceed 15% [*Wright et al.*, 2001]. Wright et al. have given a detailed description of the six-moment aerosol microphysical module. Here a brief summary relevant to the present study is presented.

[8] Advection and diffusion processes operate on the dry (nondeliquesced) aerosol. The various processes in the aerosol module are performed (with operator splitting) in the order: primary emissions, water uptake, nucleation-condensation, coagulation, dry deposition, water release, and cloud processing. Primary (particulate) sulfate emissions are characterized in terms of moments by use of the lognormal distributions given by *Whitby* [1978] representing a power plant plume. Aerosol-water equilibration is assumed to be instantaneous, and water uptake and release with changing relative humidity (RH) are calculated using a size-independent water uptake ratio, defined as $\beta_{RH} = r_{wet}/r_{dry}$, computed from the data of *Tang and Munkelwitz* [1994] for $(NH_4)_2SO_4$. New particle formation via binary H_2O-H_2SO_4 nucleation is represented using the model of *Jaecker-Voirol and Mirabel* [1989], as parameterized by *Fitzgerald et al.* [1998]. The nucleated particles are produced at three discrete sizes (r_{n1}, r_{n2}, r_{n3}) with assumed relative weightings (W_{n1}, W_{n2}, W_{n3}; $W_{n1} + W_{n2} + W_{n3} = 1$), in analogy with the three quadrature abscissas and weights [*Wright et al.*, 2001]. For this application, (r_{n1}, r_{n2}, r_{n3}) = (0.7, 3, 8 nm) and (W_{n1}, W_{n2}, W_{n3}) = (0.33, 0.33, 0.34). We have not investigated the sensitivity of our model to nucleated particle size. However, we expect little effect as the freshly nucleate particles are too small to contribute to the moments (other than particle number). Evidence for this is found in an early paper on the conventional MOM wherein the nucleated particles were assigned zero radii with negligible effect on the moments [*McGraw and Saunders*, 1984]. Nevertheless, with the QMOM it appears necessary for numerical stability to assume a narrow distribution (for the freshly nucleated particles only) so as to get the initial quadrature points. This serves to get the evolution started, whereas for a monodisperse distribution the three-point quadrature matrix would be singular. The neutralization of H_2SO_4 is not explicitly modeled, and all H_2SO_4 is treated as ammonium sulfate immediately upon condensation.

[9] The moment evolutions due to condensation, coagulation, and dry deposition are done on the basis of the quadrature abscissas and weights. The moments evolve solely by evolution of the abscissas with the weights remaining constant under condensation growth, and by evolution of the weights with the abscissas remaining constant under dry deposition [*McGraw and Wright*, 2003]. The condensation rate is the modified Fuchs-Sutugin formula [*Russell and Seinfeld*, 1998; *Kreidenweis et al.*, 1991], and the Fuchs kernel [*Fuchs*, 1964; *Jacobson et al.*, 1994] for coagulation is used. Dry deposition velocities have been calculated from the model of *Giorgi* [1986] for deposition to both ocean and land surfaces. The moment evolutions due to aqueous chemistry, rainout, and washout during the cloud period are described in section 2.4.

2.2. Transport and Emissions

[10] The advection and vertical and horizontal diffusion schemes implemented in the MAQSIP are described by *Odman and Ingram* [1996]. While these schemes are suitable for chemical species, they cannot be applied to each of the moments because the moments of a PDF are not mathematically independent quantities. For example, the aerosol PDF is a positive definite distribution whose moments must satisfy certain convexity relations and moment inequalities [*Feller*, 1971]. The best known of these is Chebyshev's inequality $\mu_2 - (\mu_1)^2 \geq 0$, but there are relations [*Feller*, 1971] connecting the higher-order moments as well. Moment sequences can fail to satisfy these relations if advected independently, as advection algorithms in CTMs are only approximate. To overcome this limitation, inherent in most advection algorithms, we perform all aerosol mixing processes in such a way that moment sequences are advected as a whole. For this purpose a moment sequence may be viewed as a vector whose components are the moments themselves. This integral treatment of moment sets has been implemented by a "linear combination" approach whereby information is saved during the updating of particle number that is

subsequently used to consistently update the higher moments as linear combinations of the moments in neighboring cells.

[11] Emissions of gas phase SO_2 and aerosol sulfate are prescribed in the model based on the 1990 EPA National Emissions Trends (NET90) Inventory. The number of layers used for emissions was limited to 14 ($\sim$2600 m) so as to not exceed a realistic maximum plume rise height [*Houyoux et al.*, 2000]. Figure 1 shows the distribution of summer SO_x (i.e., SO_2 + sulfate) emissions over the eastern United States including both surface and elevated sources. Emissions occur mainly over the heavily industrialized Ohio River Valley and the mid-Atlantic coast region. Approximately, 98.8% (by mole) of the sulfur is emitted in the form of SO_2 and 1.2% in the form of SO_4^{2-}. On the basis of the National Acid Precipitation Assessment Program (NAPAP) emissions inventory, *Dennis et al.* [1993] found that the fraction of sulfur emitted in the form of SO_4^{2-} ranged from 0.7 to 4.3% with a median of 1% for the eastern United States. The emission fraction of SO_4^{2-} employed in this study is close to the median value of *Dennis et al.* [1993].

2.3. Sulfur Chemistry

[12] The model includes a representation of gas phase oxidation of SO_2 by OH as well as aqueous phase SO_2 oxidation by H_2O_2 in cloud droplets. For OH and H_2O_2 concentrations, we use the prescribed hourly mean 3-D fields obtained from photochemical model calculations using the Carbon Bond Mechanism (version 4.2) [*Gery et al.*, 1989; *Kasibhatla et al.*, 1997b, 2000; *Kasibhatla and Chameides*, 2000] with the same meteorology. *Koch et al.* [1999] explored the importance of using prognostic H_2O_2 by comparing results with those from a run having fixed H_2O_2 fields and found that the fixed H_2O_2 simulation had typically about 5% more sulfate at the surface, 5–10% less surface SO_2, and about 10% greater deposition flux. The rate constant for SO_2 oxidation by OH is taken as 1.0×10^{-12} cm^3 molecule^{-1} s^{-1}. As this rate can vary with the temperature, the oxidation rate of SO_2 by OH calculated according to the method of *DeMore et al.* [1992] will be added in the future work. Following *Kasibhatla et al.* [1997a], we use a simplified H_2O_2 limitation scheme for the in-cloud oxidation of SO_2 by H_2O_2. Specially, we assume that if the H_2O_2 concentration within the grid box is greater than the SO_2 concentration, all SO_2 within the grid box is converted to sulfate, otherwise the amount of SO_2 converted to sulfate is set equal to the amount of H_2O_2 within the grid box.

2.4. Cloud Processes

2.4.1. Cloud Scheme

[13] The cloud types in the MAQSIP are subgrid convective cloud (precipitating and nonprecipitating) and grid-scale resolved stratiform cloud. The resolved and subgrid cloud modules were derived from the mesoscale model [MM5, *Grell et al.*, 1994] and the diagnostic cloud model in the Regional Acid Deposition Model (RADM) version 2.6 [*Chang et al.*, 1987, 1990; *Dennis et al.*, 1993; *Walcek and Taylor*, 1986], respectively. *Dennis et al.* [1993] discussed the limits of the simplified convective model originally conceived for the RADM and corrections to the RADM (version 2.6). As the resolved clouds are large scale and always occupy the full grid box, we take them as stratiform. The subgrid clouds modeled in RADM are convective and taken as cumulus. The nonconvective and convective precipitation amount outputs from MM5 were used to drive the resolved cloud and subgrid precipitating cloud, respectively, in MAQSIP. This means that only total precipitation amounts at the first layer (surface) are available but not data for each layer and that the subgrid precipitating clouds are simulated only when the MM5 indicates precipitation from its convective cloud model. In this study, we distributed the total precipitation amount to each vertical cell on the basis of a weighting function calculated according to the available information from output of MM5 as described in Appendix A. With the precipitation rate at each layer, and the condensed cloud water and rainwater reported by MM5, the resolved cloud model evaluated aqueous chemical reactions and wet deposition using the procedure described in section 2.4.2. For resolved clouds, their lifetimes were assumed to vary on the basis of the time step of the model. This means that the effect of the resolved clouds on species concentrations was calculated at each time step of the model although the meteorological driver (MM5) gave hourly output for the resolved clouds. The parameters for the resolved clouds at each time step (<1 hour) in this model were interpolated on the basis of the hourly output from the MM5. For all subgrid clouds, a 1-hour lifetime has been assumed and the influence of subgrid clouds on the species concentrations was calculated once an hour. The cloud fraction calculations for the subgrid cloud depend on cloud types and have been described thoroughly by *Dennis et al.* [1993].

2.4.2. Cloud Processing for Aerosol Evolution and Wet Deposition

[14] When the meteorological driver indicates that cloudy air is present, the aqueous chemistry routine uses gas phase SO_2 and H_2O_2 concentrations to calculate the total amount of sulfate produced in the limiting reagent approach as described in section 2.3. When cloud is formed in an air parcel, the MOM must partition the aerosol into activating and interstitial portions, and characterize each portion by a set of moments. To perform this partitioning and apportion sulfate mass among the cloud drops, we first estimate cloud droplet number by using the aerosol activation parameterization method of *Abdul-Razzak et al.* [1998], which implicitly accounts for control of maximum supersaturation by aerosol concentration and size distribution. For a single aerosol type, this parameterization method requires characterization of the aerosol PDF in terms of a lognormal distribution. The lognormal parameters N, r_g, and σ_g can be obtained algebraically from any three of the six moments; μ_0, μ_1, and μ_3 are used here. The activated fraction (N_c/N) of the aerosol is estimated with the activation parameterization method and then cloud droplet number is calculated with activated fraction and particle number. A MIDAS surrogate to the unknown PDF is retrieved from the six moments. The particle radius ($r_{c,\mathrm{eff}}$), from which to infinity integration of the surrogate PDF yields a number of particles equal to the estimated cloud droplet number, can be found. With this $r_{c,\mathrm{eff}}$, we partition the surrogate PDF into activating and interstitial portions. Then the moments of the interstitial aerosol are calculated with the surrogate PDF from 0 to

$r_{c,\mathrm{eff}}$, and subtracting these moments from the total moments yields the moments of the activating portion of the aerosol. In view of the extreme narrowing of cloud drop size distributions relative to the size distribution of the activated particles, and because aqueous reaction rates within clouds are to a good approximation proportional to cloud drop volume, we apportion the sulfate formed by aqueous phase reactions equally among the activated particles. A more detailed description is given by *Wright et al.* [2001]. After evolution of the activated aerosol, the moments of these two portions of the aerosol are summed to give the moments of the total aerosol at the end of the time step.

[15] The wet deposition rates are due to two processes: rainout (in-cloud scavenging) and washout (below-cloud scavenging). In this study, both processes are treated as first-order loss and simultaneous processes without operator splitting. For aerosols, a washout coefficient depending on retrieved r_g and σ_g was computed on the basis of calculations of *Dana and Hales* [1976] for mass washout coefficients [Figure 2 of *Dana and Hales*, 1976] with the fourth-order polynomial equation. Again, the lognormal parameters N, r_g, and σ_g are obtained from moments: μ_0, μ_1, and μ_3. SO_2 is partitioned according to Henry's Law between the gas phase, the cloud water, and the rainwater from above that will pass through the cell during the time step. H_2SO_4 and sulfate aerosol are assumed to be completely in the aqueous phase, and partitioned between the cloud water and rainwater according to their relative amounts. Details on calculation of wet deposition rates (rainout and washout) for SO_2, H_2SO_4, and sulfate aerosols are described in Appendix B. As the resolved clouds are large scale and always occupy the full grid box, we take them as stratiform. The subgrid clouds modeled in RADM are convective and taken as cumulus. The basic approach within the aerosol module is to run independent, concurrent simulations for three sets of conditions: (1) the appropriate clear-sky conditions, (2) the conditions for cumulus clouds as indicated by the subgrid cloud module, and (3) the conditions for stratiform clouds as indicated by the resolved cloud module. The results for the moments are then updated by forming a linear combination of the results obtained for the three independent simulations using the fractional cloud cover for each cloud type. It sometimes occurs in the model that even when a resolved cloud is specified by the meteorological preprocessor (MM5) to be present throughout the entire grid cell (cloud-cover fraction equal to unity), the subgrid convective cloud module (RADM) will also create a nonprecipitating cloud for some fraction of the grid cell volume. When this occurs these cloud-cover fractions are rescaled until their sum is unity. These rescaled cloud-cover fractions are then used in forming the linear combinations used for updating the moments and sulfuric acid vapor concentration, as described previously.

2.5. Base Case and Sensitivity Studies

[16] Model runs were carried out for a base case and for three sensitivity studies:

2.5.1. Case 1: Base Case

[17] In this case, the model considers all processes as described above and the fraction of sulfate (including mass and all moments) taken into rain and cloud water as 100% during cloud periods. We refer to this case as "100%" scavenging case and base case.

2.5.2. Case 2: "50%" Scavenging Case

[18] Same as case 1, but only 50% of sulfate was taken into rain and cloud water during the cloud process. Measurements of the chemical composition of the liquid water and interstitial air in warm, nonprecipitating stratocumulus clouds at various locations in the eastern United States, *Daum et al.* [1984a, 1984b] showed that the peak of the distribution of scavenging efficiencies for SO_4^{2-} was at a lower value (0.6–0.8) than for $H^+$and NO_3^- and a substantial number of samples exhibited values of scavenging efficiencies that were less than 0.5. As recommended by P. Daum (personal communication, 2001) on the basis of their measurements, the fraction of sulfate taken into cloud water during the cloud process is taken as 50%. The 50% scavenging efficiencies are applied uniformly to all six moments. We refer to this sensitivity case as 50% scavenging case. Comparisons of simulation results of "100" and 50% cases permit examination of sensitivity of the simulation results to fractional uptake.

2.5.3. Cases 3 and 4: Doubling the Condensation Rate

[19] In these sensitivity studies, we doubled the condensation rate of H_2SO_4 onto the sulfate aerosol for both "50" and "100%" cases to account for condensation onto other aerosols. As fine particle mass concentration over the eastern United States is about 60% sulfate [*Sisler and Malm*, 2000], this may account for the effect of other aerosols (organics, sea salt, dust, and others) under the assumption that other aerosols provide aerosol surface area for condensation equal to that of the sulfate aerosol. This reduces the concentrations of gaseous sulfuric acid and hence the rates of nucleation and coagulation.

2.6. Retrieval of Modeled Size Distributions

[20] The modeled size distributions were retrieved by the RMST [*Yue et al.*, 1997; *Wright et al.*, 2002] on the basis of the six moments from the model. In the RMST retrieval, we used 19 nonuniform bins with radius boundaries of 0.01, 0.02, 0.03, 0.04, 0.05, 0.06, 0.07, 0.085, 0.10, 0.125, 0.15, 0.20, 0.25, 0.35, 0.45, 0.60, 0.75, 1.00, 1.25, and 1.75 μm. The last 15 bin structures of the RMST retrieval are chosen to be the same as those of a Passive Cavity Aerosol Spectrometer Probe (PCASP). The basic idea of RMST is to find a retrieved size distribution (19 size bins) whose calculated six moments have a minimum deviation from the modeled six moments. The bin structure, number of bins, number of solutions, and convergence tolerance are the most important parameters. In this application, the retrieved size distribution is obtained by averaging 20 solutions with 1% tolerance.

3. Simulation of Sulfate Aerosols and Model Evaluation Over the Eastern United States

[21] The sulfate aerosol concentrations and size distributions over the eastern United States strongly depend on the emissions and chemical-physical atmospheric processes. Over the eastern United States, the surface sulfate concentrations show a strong seasonal cycle with maxima in the summer and minima in the winter [*Shaw and Paur*, 1983]. The simulation results of *Kasibhatla et al.* [1997a] found that the column SO_4^{2-} burden over the eastern North

America was ~15 mg m^{-2} in summer, much higher than that in winter (~6 mg m^{-2}) because of increased photochemical production of oxidants. As sulfate is the most important component of aerosols and sulfate aerosol concentrations (both natural and anthropogenic) are the greatest over the eastern United States in summer, the ability to simulate the variability in sulfate aerosol properties during the summer will provide a good test for the performance of the model.

3.1. Measurements Used for Model Evaluation

[22] A comprehensive performance evaluation of the aerosol module in a 3-D air quality model requires an extensive data set on aerosol properties. The Southeastern Aerosol and Visibility Study (SEAVS) measured sulfate mass concentration, aerosol number concentration, and size distributions at the Great Smoky Mountains (GSM) National Park during July and August 1995 [*Andrews et al.*, 2000; *Ames et al.*, 2000]. To use this data set, we have run the 40-day simulation from 1200 UT on 19 July to 1200 UT on 28 August 1995. These measurements and four other data sets suitable for model evaluation during this period are briefly described below.

[23] The data sets for the sulfate aerosols are as follows: (1) data from the SEAVS experiment conducted from 15 July through 25 August 1995, at Look Rock Ridge (84°W, 36°N; elevation 900 m) at the GSM [*Andrews et al.*, 2000; *Ames et al.*, 2000]. The mean sulfate mass concentrations were determined using Teflon filter as a collection method with inlet size cuts of 2.1 μm (IMPROVE sampler) over 12-hour daytime sampling periods (0700 hours to 1900 hours EDT) [*Ames et al.*, 2000]. The aerosol number size distributions between 0.05 and 1.25 μm radii with 34 bins were determined by an Active Scattering Aerosol Spectrometer (ASASP-X) with a sampling time of at least 15 min [*Ames et al.*, 2000; S. Kreidenweis et al., private communication, 2002]. If more than one measurement was available in an hour, the first measured size distribution was used to represent the measurement in that hour. A total of 105 observed size distributions, with RH < 40% to represent the dry aerosols [*Ames et al.*, 2000], was used to compare with the model results. Note that by assuming that the aerosol is always dry at RH < 40%, we will sometimes underestimate particle size at low RH. (2) The observed sulfate mass concentrations from the Clean Air Status and Trends Network [CASTNET, *Holland et al.*, 1999]. Teflon filters were normally exposed for 1-week intervals (Tuesday to Tuesday) to collect aerosol for sulfate mass concentration analysis. (3) The observed sulfate mass concentration data from the IMPROVE program. Two 24-hour samples were collected on Teflon filters each week, on Wednesday and Saturday, beginning midnight local time [*Sisler and Malm*, 2000]. (4) Vertical profiles of the aerosol number size distributions determined during the Southern Oxidants Study (SOS). Size distributions for particle radii in 15 size bins between 0.05 and 1.75 μm were determined by a PCASP over Nashville, TN, from 24 June to 20 July 1995 [*Hubler et al.*, 1998]. (5) The aerosol size distributions at Black Mountain (35.66°N, 82.38°W, elevation 951 m), Mt. Mitchell State Park, North Carolina. Size distributions between 0.008 and 0.3 μm radii with 50 size bins were determined by the Thermo Systems Inc. (TSI) Differential Mobility Particle Sizer (DMPS) [*Yu et al.*, 2000, 2001]. As heating was applied to the aerosol sampled by the PCASP and DMPS, it is assumed that the results are representative of the dry aerosol size distributions. The sulfate mass concentrations were calculated under the assumption that particles were composed of ammonium sulfate. SO_2 mixing ratios are also available in the above studies except those on Black Mountain. Observations at sites which were not classified as rural sites or were not located at least five grid boxes from the nearest model boundary were excluded. In some small number of cases where two or more stations were located in a single grid cell, the mean observation was used.

[24] For the comparison of wet sulfate deposition, two data sets from the National Atmospheric Deposition Program [NADP, see *Lynch et al.*, 1995] and EPA CASTNET [*Holland et al.*, 1999] are used. Both NADP and CASTNET measure sulfate wet deposition with weekly resolution (starting and ending at 0900 LT on Tuesdays). In summary, the observed sulfate mixing ratios at 60 stations, SO_2 mixing ratios at 45 stations, and wet sulfate deposition at 117 stations were used to evaluate the performance of the model over the eastern United States. Reported concentrations of sulfate and SO_2 in air were converted from the original units to mixing ratios in units of parts per billion (ppb = nmol mol^{-1} air) as this quantity has the advantage of being independent of pressure and temperature [*Schwartz and Warneck*, 1995]. Figure 7 shows the locations of the stations whose observations were used in this study over eastern United States.

3.2. Initial and Boundary Conditions

[25] The model was initialized by using the model itself to generate initial conditions. First, mixing ratios of gaseous SO_2 and H_2SO_4 for all cells were set to 10^{-3} and 10^{-4} ppb, respectively, and the six moments of aerosol size distribution for all cells were calculated according to the results for the marine background aerosol case from Table 7.3 of *Seinfeld and Pandis* [1998], i.e., N_1 = 133 cm^{-3}, D_{p1} = 0.008 μm (geometric mean diameter), $\ln(\sigma_{g1})$ = 0.657 (geometric standard deviation); N_2 = 66.6 cm^{-3}, D_{p2} = 0.266 μm, $\ln(\sigma_{g2})$ = 0.210; N_3 = 3.1 cm^{-3}, D_{p3} = 0.58 μm, $\ln(\sigma_{g3})$ = 0.396. Under the assumption that the aerosol consisted of ammonium sulfate, the sulfate mixing ratio was 0.42 ppb for this marine background aerosol case. The boundary conditions were the same as these initial conditions. The model was run for the 40-day period (1200 UT on 19 July to 1200 UT on 28 August 1995) with the MM5 meteorological conditions. Then we used the results of 40-day simulation as the initial conditions for the next 40-day simulation and the boundary SO_2 mixing ratio was set to 0.17 ppb for this new run. This approach was taken so as not to bias the model to low concentrations that would result if the model run were initialized with low background concentrations.

3.3. Evaluation of Model and Discussions

3.3.1. Time Series Comparisons at the GSM and at the Black Mountain, North Carolina

[26] This section compares time series of modeled and observed moments, mass concentration, and size parameters. Figure 2 shows the time series of observed and modeled sulfate mass and the synoptic conditions at the GSM location during the SEAVS period [*Sherman et al.*,

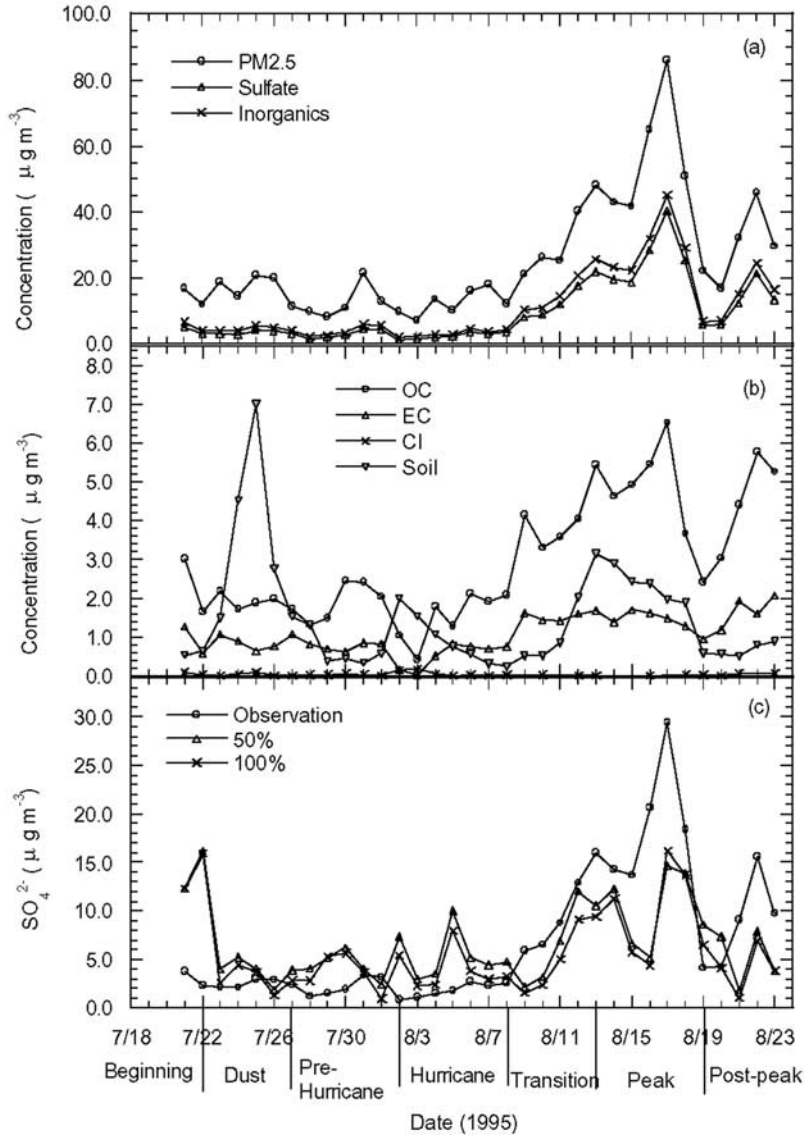

Figure 2. (a) The time series of the observed mass concentrations of $PM_{2.5}$ mass, sulfate, and inorganics ($SO_4^{2-} + NO_2^- + NO_3^- + NH_4^+ + Na^+ + Cl^-$); (b) OC, EC, Cl^-, and soil (2.14*Si + 2.89*Al + K + Ca + Fe + Mg) mass [*Sherman et al.*, 1997]; (c) the time series of observed and modeled sulfate at the GSM during the SEAVS period.

1997; *Ames et al.*, 2000]. The dominant synoptic feature during this period was Hurricane Erin, which made landfall around 2 August 1995. As shown in Figure 2c, the model captured the buildup of observed sulfate mass from 9 to 13 August, a dip during 15–16 August, and a peak during 17–18 August. However, the model underpredicted slightly sulfate mass peak after the Hurricane and overpredicted slightly the sulfate mass concentrations before and during the Hurricane Erin (Figure 2c).

[27] For comparison of aerosol number concentration, moments, and size parameters, one should bear in mind that the model simulates sulfate only whereas the observed moments and size distributions include all aerosol species. Figure 3 shows that there were large variations of observed six moments at the GSM during the SEAVS period. The observed moments except μ_0 were very high during the dust (23–26 July) and peak concentration (13–19 August) periods, especially for μ_4 and μ_5, when compared to other periods. As compared to the observations in Figure 3, the model generally performs much better on the low moments (μ_0 and μ_1) than high moments (μ_4 and μ_5) at the GSM. The mean modeled number concentrations are 1516 cm^{-3} for the base case, somewhat higher than the mean observed number concentration (1139 cm^{-3}). The measurements determined the number size distributions only between 0.05 and 0.125 μm, leading to possible underestimate of the actual number concentration (0th moment). The first panel of Figure 3 for the number concentration (μ_0) shows that the model has similar magnitude to the observations and captured the increase trends of the observed number concentrations during 10–17 August at the site. The model seriously underpredicts the high moments, especially for μ_4 and μ_5, during the periods of dust (23–26 July) and high concentrations (13–19 August). These underpredictions are

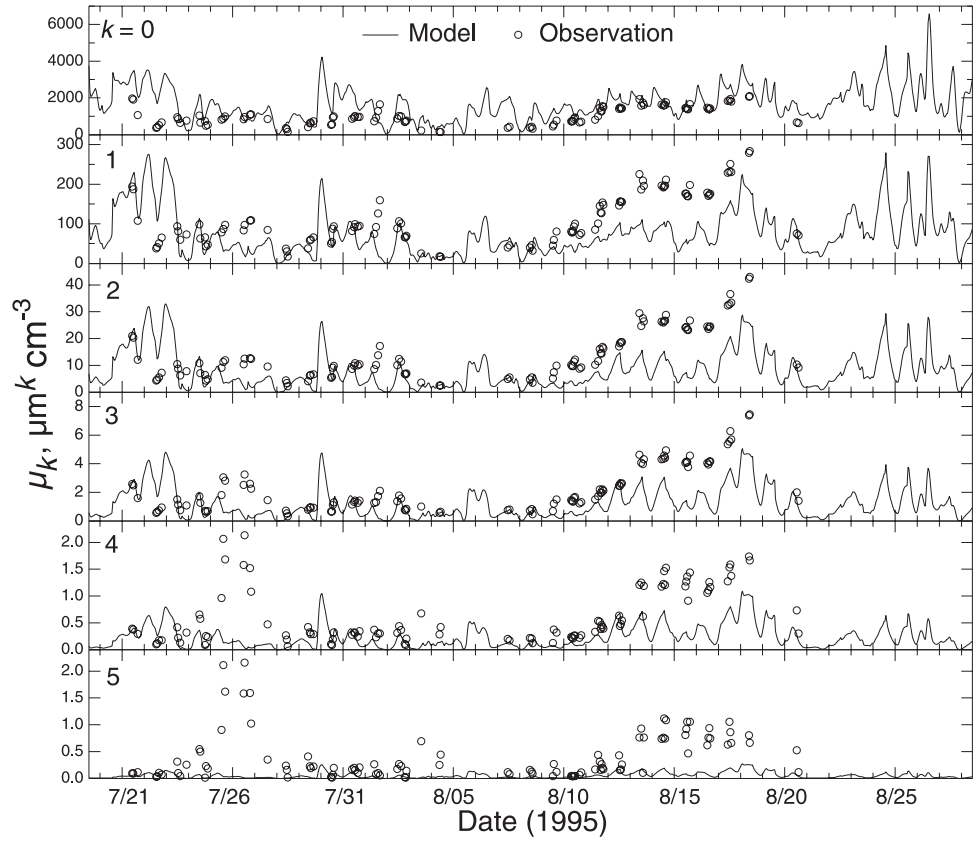

Figure 3. Time series of modeled and observed six moments at the GSM. The observed six moments were calculated on the basis of measurements obtained by S. Kreidenweis et al. (private communication, 2002) [*Ames et al.*, 2000].

attributed to the contributions of large particles of aerosol species other than sulfate in the observed particles as analyzed below. The soil mass concentration of the fine aerosol (diameter < 2.5 μm) was the highest for the whole study during the dust event, indicating the likely presence of large particles [*Sherman et al.*, 1997]. The organic carbon (OC) concentrations increased dramatically during the transition and peak period (8–18 July) as shown in Figure 2.

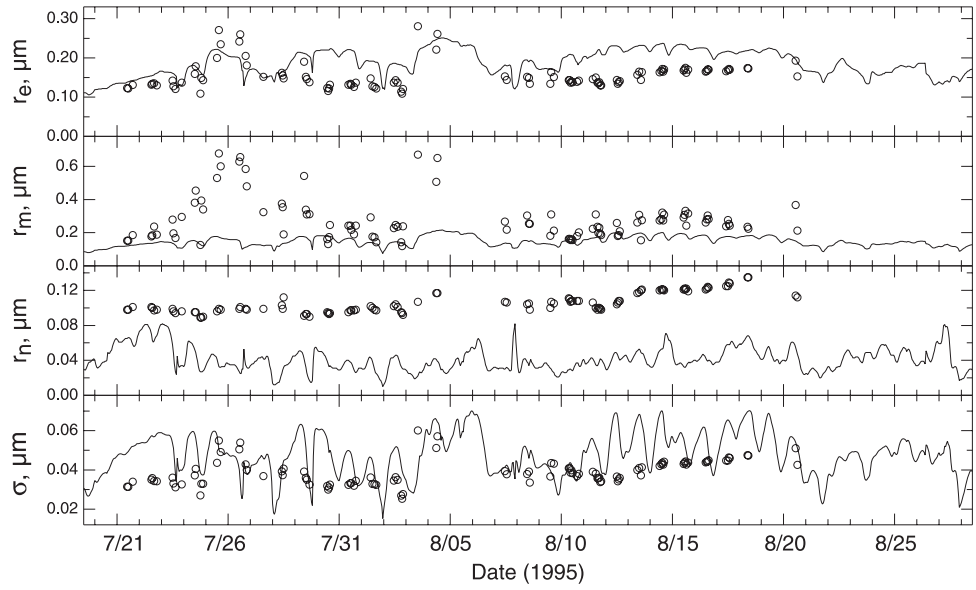

Figure 4. Time series of modeled and observed effective radius (r_e), mass mean radius (r_m), number mean radius (r_n), and standard deviation of radius at the GSM. Circles and solid lines represent observation and model, respectively.

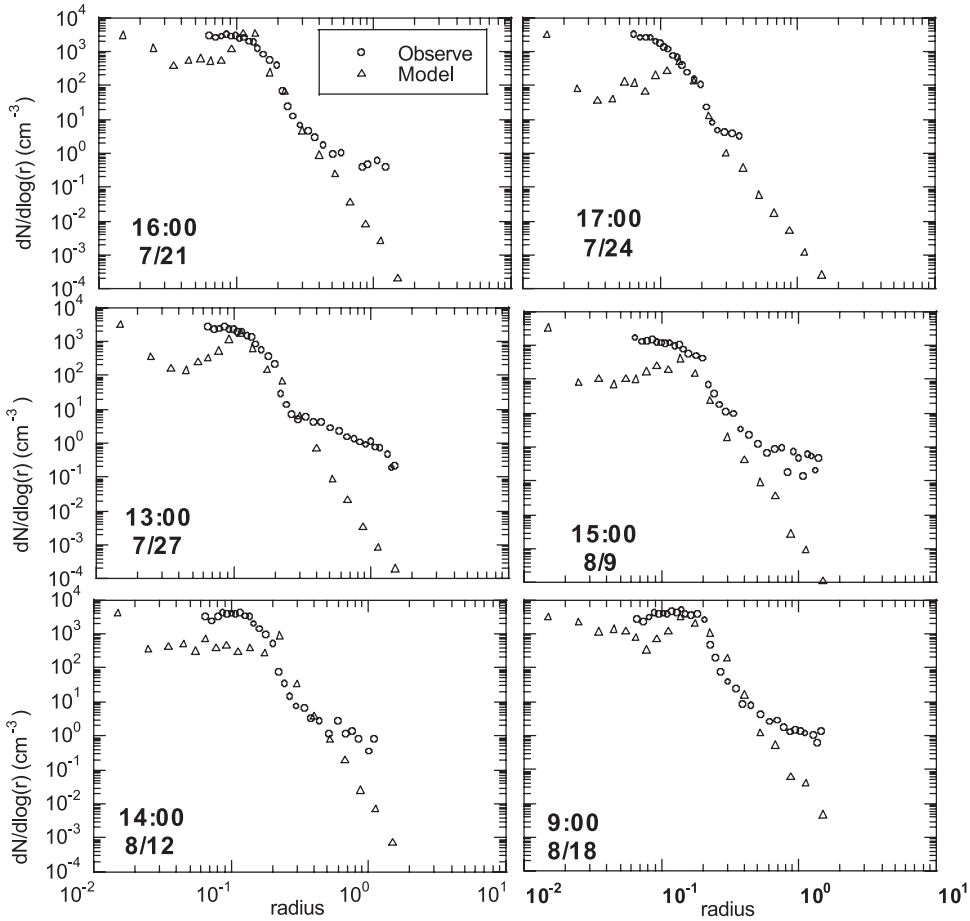

Figure 5. Comparisons of the observed and modeled size distributions at different times on the GSM during SEAVS period. Note that the modeled size distributions were retrieved by the RMST method on the basis of the modeled moments (see explanation in the text).

[28] The number concentrations and number mean radii are determined mainly by the particles at the small size range (nucleation mode) whereas effective radii and mass mean radii are determined mainly by the particles at the large size range (accumulation and coarse modes). For example, *Woo et al.* [2001] found that approximately 89% of the total number of particles were smaller than 0.05 μm radius, and 26% were smaller than 0.005 μm radius on the basis of aerosol size distributions in 0.0015–1.0 μm radius range measured every 12 min for 24 months beginning August 1998 in Atlanta, GA. Therefore it is extremely difficult to simulate the number concentrations and size distribution, and this is a big challenge for modeling aerosol evolution. The work of *Whitby* [1978] demonstrates the strong tendency for the nucleation, accumulation, and coarse particle modes to separate when the particle distribution function is transformed in terms of number, surface area, and volume coordinates. Specifically, the nucleation mode is revealed on a number distribution plot, the accumulation mode on a surface area distribution plot, and the accumulation and coarse modes, which make similar but separate contributions, on a plot of the particle volume distribution. The radial moments for each of these transformed distributions are given in terms of moment ratios that utilize just the four lowest-order radial moments of the original (untransformed) particle distribution function. These are the number mean radius ($r_n = \mu_1/\mu_0$), the surface area mean radius (μ_3/μ_2), which equals effective radius (r_e), and volume mean radius (μ_4/μ_3), which equals mass mean radius (r_m). Taken together, these moment ratios provide a powerful, targeted indicator of model performance for representing the different Whitby modes. Figure 4 shows the time series of these modeled and observed moment ratios (r_e, r_n, and r_m) at the GSM during the SEAVS. The observed r_n values are systematically higher than the modeled values over the whole period and the observed r_m values are also systematically higher than the modeled values during the dust and peak periods when other aerosols made a substantial contribution to the total aerosol population (Figures 2a and 2b). In contrast, both mean modeled r_e (0.159 μm) and size standard deviation σ (0.050 μm) were close to the observations (r_e = 0.155 μm and σ = 0.039 μm) as indicated in the time series of Figure 4. This is in agreement with the expectation that the sulfate model provides a good representation of the accumulation mode and most of surface areas of the particles have been represented by the modeled sulfate as indicated below.

[29] The modeled size distributions were retrieved by the RMST [*Yue et al.*, 1997; *Wright et al.*, 2002] on the basis of the corresponding six moments from the model. Figure 5

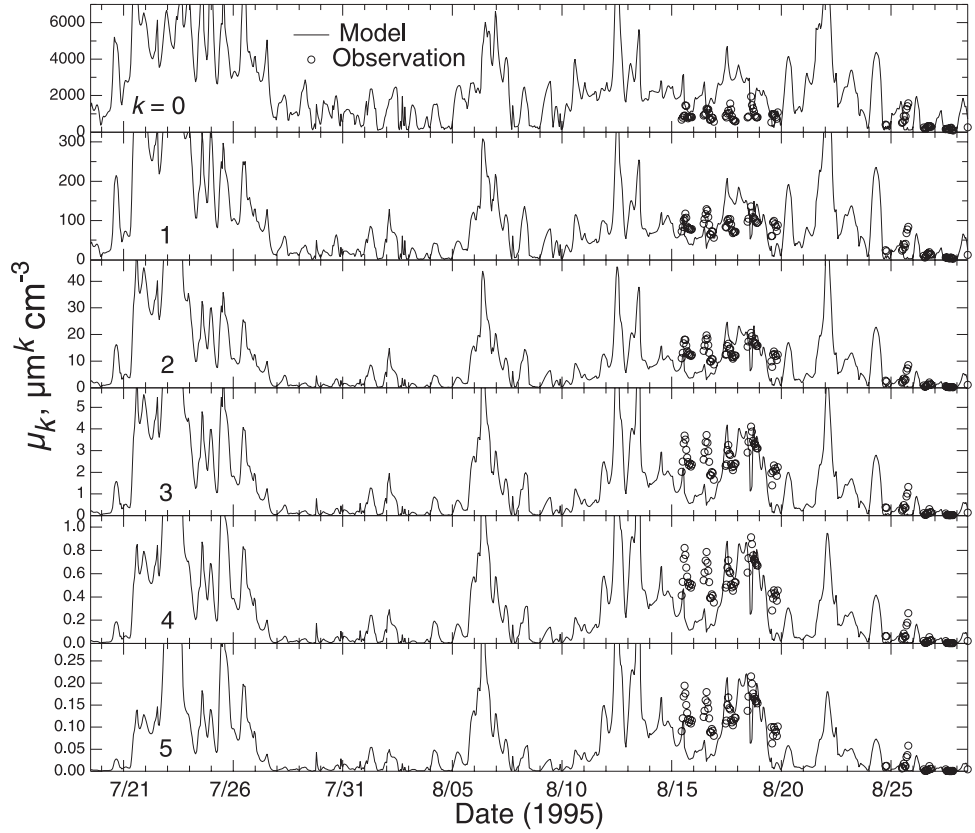

Figure 6. Time series of modeled and observed six moments at the Black Mountain in the summer of 1995.

shows comparisons of modeled and observed size distributions for some cases at the GSM. Note that ASASP-X measured aerosol number size distributions only between 0.05 and 1.25 μm radii. As can be seen, the model successfully captured the observed size distributions in the accumulation mode between 0.10 and 0.40 μm radii, with some underestimates especially for large particles (radius > 0.5 μm) and small particles (radius < 0.1 μm). It should be recalled, however, that the sulfate is expected to exhibit dry radius smaller than 0.5 μm, whereas the larger particle radii are expected to be dominated by other species. This may account for the departure above this radius. This is in agreement with the recent modeling study of global mixed aerosol fields of *Wilson et al.* [2001], who found that the accumulation mode near the surface is dominated by the sulfate mode in the continental areas.

[30] The observed small particles (radius < 0.1 μm) and large particles (radius > 0.5 μm) undoubtedly include the contributions of aerosol substances other than sulfate. There were other significant aerosol components at the GSM during SEAVS period as shown in Figures 2a and 2b [*Sherman et al.*, 1997]. The mean concentrations of $PM_{2.5}$, $(NH_4)_2SO_4$, inorganics, OC, elemental carbon (EC), Cl^-, and soil were 25.38, 9.40, 11.28, 2.98, 1.08, 0.04, and 1.47 μg m^{-3}, respectively. This indicates that ammonium sulfate and TOC (OC + EC) contributed 37 and 16% for $PM_{2.5}$ mass, respectively, at the GSM during the SEAVS (Figures 2a and 2b). This points out the important contributions of nonsulfate aerosols to the observed particles. Nucleation events apparently attributable to organics have been frequently observed in the forested region [*Kulmala et al.*, 1998; *Kavouras et al.*, 1998] and industrialized agricultural regions [*Birmili and Wiedensohler*, 1998]. In the chemical analysis of the particles smaller than 0.25 μm radius in connection with the increase of the Aitken nuclei over a forested area, *Kavouras et al.* [1998] found the existence of organic acids (such as pinonic, formic, and acetic acids), which are formed as oxidation productions of gaseous monoterpenes emitted by the forest. The importance of the anthropogenic hydrocarbons in the formation of secondary organic aerosol was also emphasized by *Odum et al.* [1997]. Organics have been found to contribute substantially to aerosol optical depths over the eastern coast of United States [*Hegg et al.*, 1997]. The results of Figure 5 can be interpreted as suggesting the presence of nonsulfate particles in both radius < 0.1 μm (nucleation mode) (perhaps organics, which are heavy in the region as shown in Figure 2b) and radius > 0.5 μm (perhaps organics and soil) that are not included in the sulfate model. This is consistent with the previous analyses for the moments in Figure 3 and size parameters in Figure 4. Discrepancy between model and observations might also arise from inaccuracy in the treatment of nucleation and of primary sulfate emissions.

[31] Figure 6 shows the time series of modeled and observed six moments at Black Mountain, NC, during 15–28 August 1995. The model captures the general magnitudes of observed six moments with better performance on μ_1 and μ_2. There are similar explanations for the discrepancy between the model and observations for size parameters at Black Mountain as those at GSM when we

retrieve the size distributions on the basis of the modeled six moments (not shown). Note that the TSI DMPS measured aerosol particles only over the radius range from 0.008 to 0.3 μm at Black Mountain as mentioned before, and the Black Mountain site (36°N, 82°W) is close to the GSM (36°N, 84°W).

3.3.2. Comparisons With the Regional Observations and Wet Deposition Over the Eastern United States

[32] Figure 7a shows the spatial distribution of ratios of modeled to observed mean values at each station during the 40-day simulation over the eastern United States for the base case. The model overestimated the SO_4^{2-} mixing ratios in some stations of the southeast but underestimated them in all stations of the northeast. For the 50% case, the underestimation of sulfate mixing ratios in the northeast was improved but the overestimation of sulfate mixing ratios in southeast was increased (Figure 7b). Figure 8 shows scatterplots of model versus the individual concentration measurements for sulfate and SO_2 mixing ratios and wet deposition fluxes. Following *Kasibhatla et al.* [1997a, 1997b], we calculated the percentages of comparison points whose model results were within a factor of 2 of the corresponding measurements for each parameter. The results are listed in Table 1. The domain averages for the comparison points were also calculated. As can be seen, about half of the observed sulfate mixing ratios were simulated to within a factor of 2, and the domain average of the modeled sulfate mixing ratios for the base run was 13% lower than the observation. Only ~25% of the sulfate wet deposition amounts were simulated to within a factor of 2, and the domain average of the model results was 76% higher than the observation for the base run. Although the modeled domain average of sulfate wet deposition for the 50% case was close to the observations (25% overestimation) (Table 1), the 50% case did not improve the model performance on the wet deposition spatially as shown in Figures 7d and 8. The model seriously overpredicted the sulfate wet deposition at most stations over the middle part of the domain (Figures 7c and 7d). Overprediction of sulfate wet deposition may be one of the reasons leading to underprediction of sulfate mixing ratios over the northeast (Figure 7a). The scatterplot of Figure 8 indicates that the model overpredicted sulfate wet deposition more when the observed sulfate wet deposition was less than 0.1 mmol m^{-2} $week^{-1}$. Inspection of Figures 7 and 8 shows that most of locations where ratios of modeled to observed mean wet deposition was larger than 3.0 in Figures 7c and 7d were locations of low sulfate deposition. As noted by *Benkovitz and Schwartz* [1997], departure of modeled and observed values may not be attributed entirely to performance of the model because the observed values at a station are not necessarily representative of the grid cell as a whole and may be not suitable for evaluation of the model, which means to represent the mean values over the grid cell. In addition to the problem of the representativeness of the observations at a single location for the grid cell as a whole, the discrepancy between the modeled and observed wet deposition can be due to inaccuracy in the representation of locations and amounts of precipitation in the meteorological forecast model (here, MM5) that drives the chemical transport model and in the representation of wet removal processes [*Seaman*, 2000]. Discrepancies between model and observations might be due also to errors in boundary conditions, especially near the western edge of the model domain. Nonetheless, these considerations suggest a need to improve the accuracy of wet processes in the model.

[33] For the sensitivity study with the doubled condensation rate, the domain averages of the modeled SO_4^{2-} mixing ratios for the 40-day simulation period were about 15% lower than for the base case (Table 1), and sulfate wet deposition about 7% higher, resulting in decreased overall model skill compared with observations. These changes are attributed to a shift in sulfate mass loading from the nucleation mode to the accumulation mode (diameter 0.1–1.0 μm). Most of the sulfate aerosols, both in ambient and in present model, are located in the accumulation mode, whereas sea salt, dust, etc., which are not included in the model, are in the coarse mode, which would contribute little to surface area. Evidently, the surface area for condensation is already accurately represented by the modeled sulfate without inclusion of coarse mode aerosol. This may be the major reason why a doubling of the condensation rate to account for aerosol species other than sulfate results in a decrease in model performance. As the accumulation mode is more efficiently removed by wet deposition than the nucleation mode, shifting sulfate from the nucleation mode to the accumulation mode enhances the removal rate.

[34] It was found that the model performs better on the mean results of the 40-day period than on individual measurements. For instance, ~60% of the observed mean sulfate mixing ratios and ~53% of observed mean wet sulfate deposition were simulated to within a factor of 2, higher than those of the individual measurements for the base case (Table 1). These results are in agreement with the study of *Dennis et al.* [1993], who found that the absolute difference between observations and model results decreased rapidly for successively longer averaging period because of temporal noise in the data set. It also probably means that the location of the material is displaced because of inaccuracies in the wind field of the meteorological driver, which would tend to average out.

[35] The model systematically overestimated the observed SO_2 mixing ratios, as shown in Figure 8. Only 22% of the observed SO_2 mixing ratios were simulated to within a factor of 2, and the modeled domain average was 138% higher than the observations (Table 1). Preliminary evaluation results of EPA's Models-3 CMAQ also found that SO_2 predications were biased high by a factor of 2 [*Mebust et al.*, 2003; R. Dennis, personal communication, 2002]. The overpredictions of SO_2 were caused mainly by the nighttime overestimation of SO_2 on the basis of comparison of hourly measurements of SO_2 from AIRS in 1990 with the CMAQ results (R. Dennis, personal communication, 2002). A possible reason is the model's coarse vertical resolution that cannot adequately resolve sharp nocturnal gradients near the surface (J. Pleim, personal communication, 2002). The overestimation of nighttime SO_2 will not lead to substantial overestimation of gas phase oxidation of SO_2 during nighttime but may lead to overestimation of aqueous phase oxidation. At the GSM during the SEAVS period, we also found that the average of the model results for SO_2 (2.23 ppb) was much higher than the mean

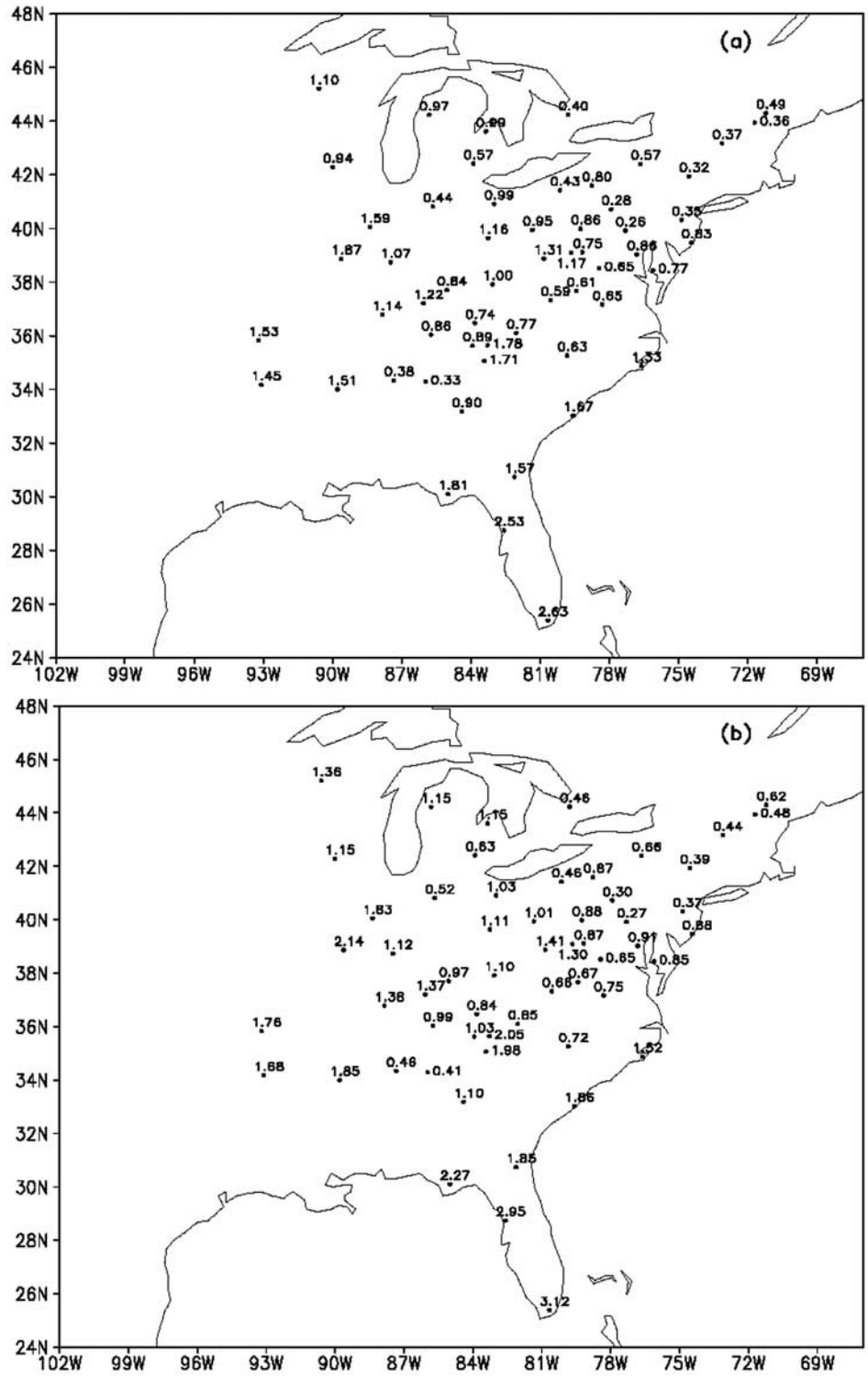

Figure 7. Ratios of the modeled to the observed variables at individual grid box locations during the period 19 July to 28 August 1995 over the eastern United States. Those for mean sulfate mass concentrations are shown in (a) 100% and (b) 50% cases. Those for mean wet sulfate deposition fluxes are shown in (c) 100% and (d) 50% cases.

observed SO_2 concentration (0.31 ppb) measured by the IMPROVE (filter sampler of the National Park Service (NPS)) and that (0.92 ppb) measured by the Harvard-EPA annular denuder system (using HEADS) during the SEAVS period *[Andrews et al.*, 2000]. *Andrews et al.* [2000] ascribed the systematically lower SO_2 value (0.31 ppb) measured by the IMPROVE to absorption of SO_2 by the 8-foot aluminum inlet tube used in the IMPROVE

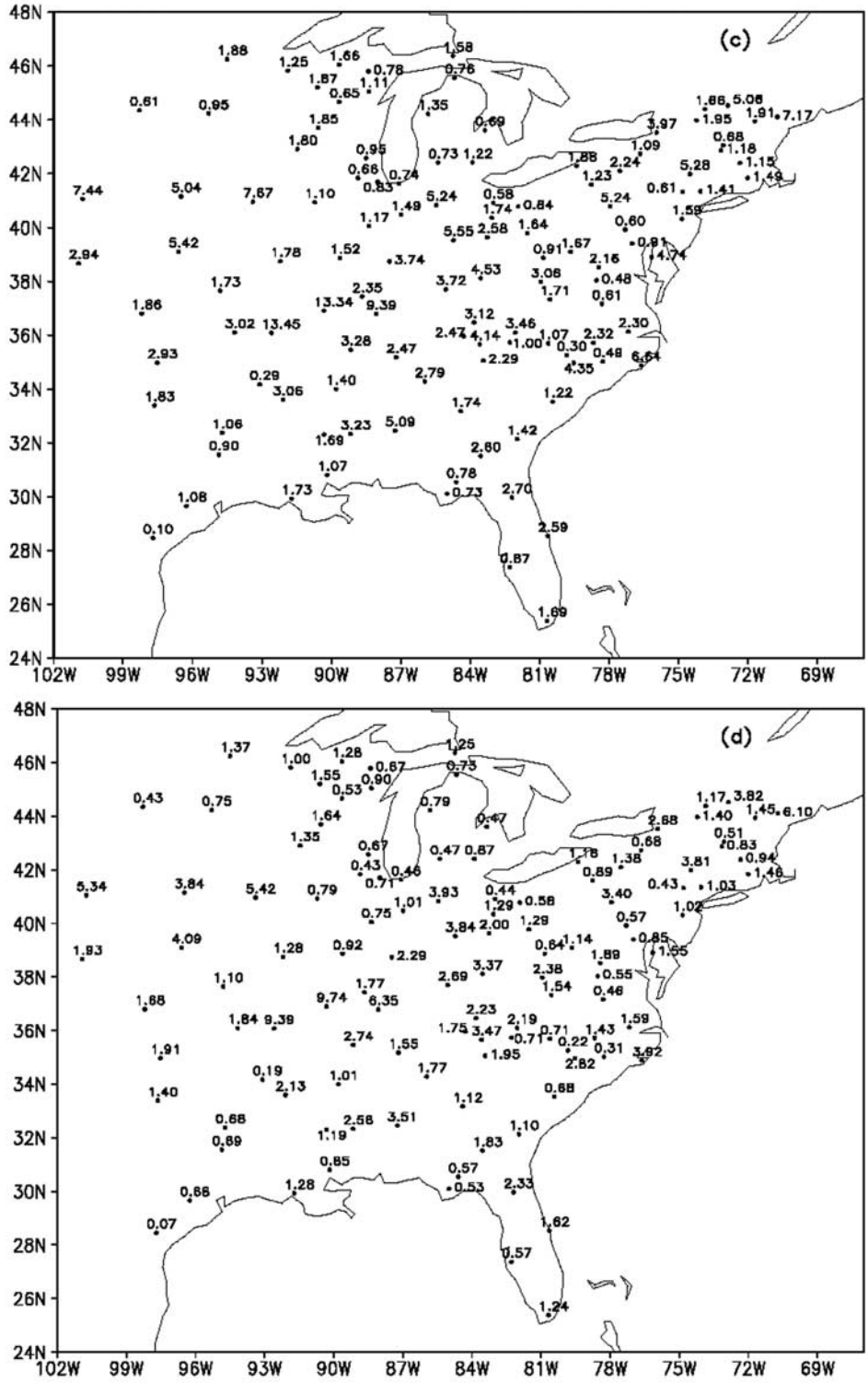

Figure 7. (continued)

sampler. This result suggests that some systematically lower SO_2 values from measurement methods may also be one of the reasons that lead to low observed SO_2 values compared to the model. SO_2 mixing ratios are also overpredicted in several global models [*Kasibhatla et al.*, 1997a, 1997b; *Barth et al.*, 2000; *Chin et al.*, 2000]. Additional possible reasons for the overestimation of SO_2 mixing ratios have been suggested: (1) additional heterogeneous mechanisms for the oxidation of SO_2 in the boundary layer and (2) nonrepresentative locations and elevations of surface observation sites. Most of the SO_2 is released from stacks above local shallow inversion layers,

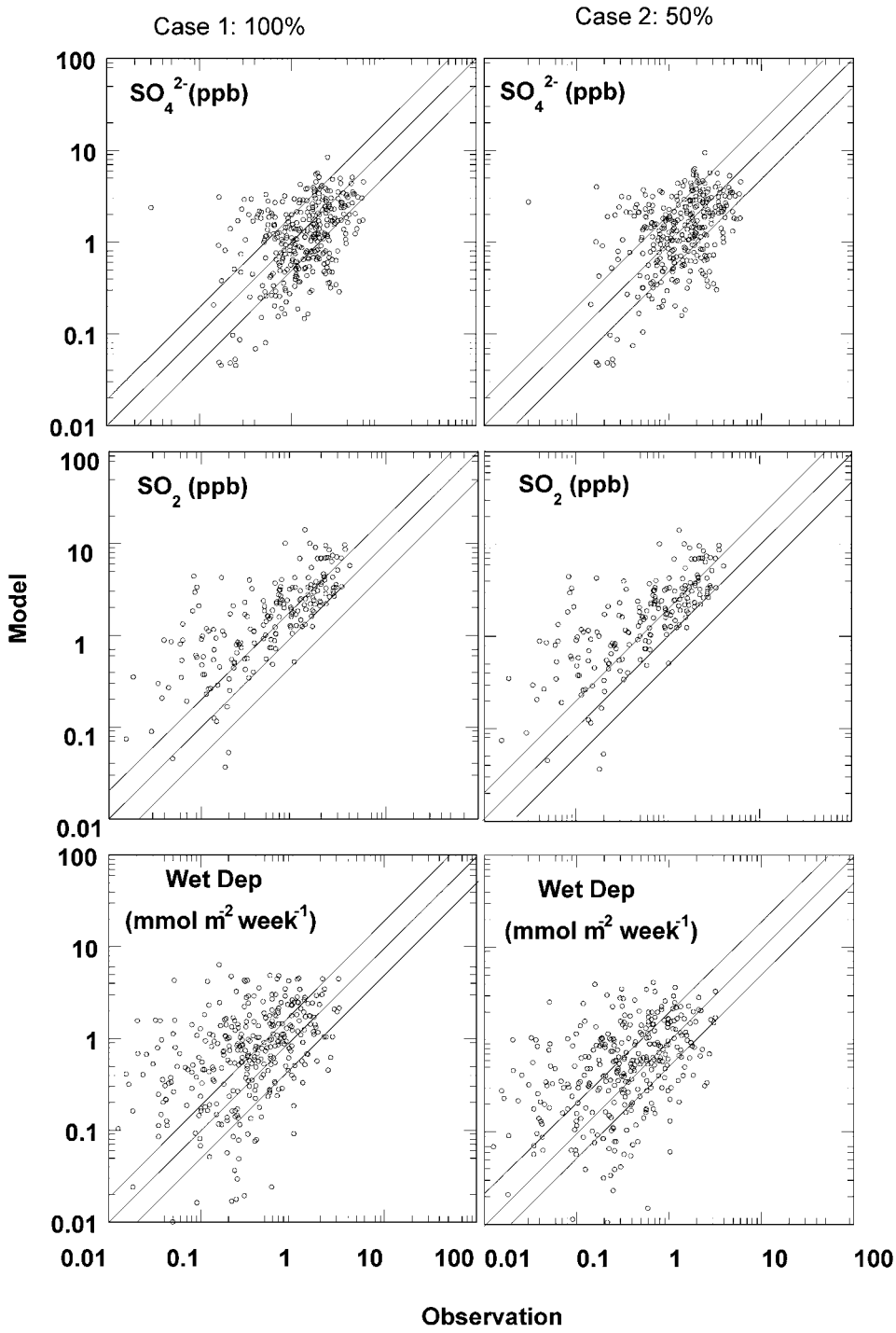

Figure 8. Comparisons of simulated and observed mean SO_2 and SO_4^{2-} mixing ratios and total wet deposition fluxes for the 100 and 50% model simulations for individual measurements during 19 July to 28 August 1995 (40 days). The 1:1, 2:1, and 1:2 lines are shown for reference.

with the observation stations located close to the surface below the inversions.

3.3.3. Comparisons of Vertical Profiles of Mass and Number Concentrations and Size Distributions With Measurements Over Nashville, Tennessee

[36] Comparisons of modeled and observed vertical profiles of sulfate mass concentrations and size parameters over Tennessee provide an assessment for the ability of the model to represent vertical structure of aerosol properties. In this study, the data of two periods (period 1: 1400 UT-1800 UT on 19 July 1995 and period 2: 1200 UT-1600 UT on 20 July 1995) from the SOS experiment over Nashville, TN, are used to compare with the model results of the base case. In order to compare the modeled and observed vertical profiles, the observed and modeled size distribution data were grouped according to the altitudes and longitudes and

Table 1. Statistical Summaries of the Comparisons of Model Results With Observations Over Eastern United States[a]

	⟨C⟩			Within Factor of 2, %	
Parameters	100%	50%	OBS	100	50
SO_2, ppb	2.62	2.62	1.10	22	22
SO_4^{2-}, ppb	1.63	1.83	1.87	46	56
[b]SO_4^{2-}, ppb	1.40	1.61	1.87	45	46
Wet deposition	0.97	0.69	0.55	25	32
[b]Wet deposition	1.04	0.74	0.55	24	31

[a]⟨C⟩, grand average, percentages (%): are the percentages of the comparison points whose model results are within a factor of 2 of the measurements. Unit of wet deposition is mmol m^{-2} $week^{-1}$. 50, 100%, and "OBS" represent the model results of 50 and 100% cases, and observations (see text).

[b]For the cases with doubled condensation rate.

latitudes of the observations, and corresponding layer heights and longitudes and latitudes of the model grid cells for each period. The corresponding mean aerosol properties and SO_2 mixing ratios were calculated for each layer for each period over the whole study region.

[37] Figures 9 and 10 show the modeled and observed vertical profiles of mean sulfate mixing ratios, number concentrations, r_e, r_m, r_n, and SO_2 mixing ratios as a function of height (pressure) over Tennessee for the periods 1 and 2, respectively. For period 1, the model generally captured the vertical variation patterns of the observed sulfate and SO_2 mixing ratios, number concentration, and r_n as shown in Figure 9, especially for the highest SO_2 mixing ratio in the plumes at around 910 hPa. For period 2, the model captures the vertical variation patterns of sulfate mixing ratios and r_n well but does poorly for other parameters as shown in Figure 10. Specifically, the model underpredicted the sulfate mixing ratios at low layers and high layers for both periods (Figures 9b and 10b). The model overpredicted SO_2 mixing ratios at low model layers for both periods but did not capture the observed SO_2 peak at around 910 hPa for period 2 (Figure 10f). This is consistent with the observation made in section 3.3.2 that the model underpredicts the sulfate slightly but overpredicts SO_2 by a factor of 2 at the ground layer.

[38] Figures 9d and 10d indicate that the modeled mass mean radii are systematically smaller than the corresponding observations for both periods. As the observed aerosol size distributions are available between 0.05 and 1.75 μm particle radius in 15 size bins measured by PCASP, we compared the mean observed size distributions with the surrogates to the size distributions retrieved by the RMST [*Yue et al.*, 1997; *Wright et al.*, 2002] on the basis of the corresponding mean six moments from the model. Figure 11 shows the examples of the comparisons of mean observed and modeled size distributions at the layers 2 (982 hPa), 7 (943 hPa), and 12 (822 hPa) for the two periods. In most cases, the model has successfully captured the observed size distributions in the middle six bins of accumulation mode (e.g., bins with radius boundaries of 0.10, 0.125, 0.15, 0.20, 0.25, 035, and 0.45 μm) which were determined mainly by sulfate aerosol. This result is in agreement with the results obtained at the GSM (Figure 5) and with the recent finding of *Brock et al.* [2002] over Nashville during the SOS' 99 field mission that sulfate contributed most of the mass of aerosol particles in the plumes from coal-fired power generation stations over Nashville on the basis of measurements of submicrometer particle size distributions in the plumes and calculations using a numerical plume photochemistry model. *Husar et al.* [1978] also showed that sulfate was a predominant component of aerosol particles formed in power plant plumes. Figure 11 shows that the retrieved number concentrations at radii larger than 0.50 μm are systematically lower than the observations for all layers, like at the GSM (Figure 5). However, the model does not underpredict the observed particles in the small size range like it does at the GSM. For the SOS Nashville/Tennessee Field Intensive, one of the major goals was to examine the role of power plant plumes in oxidant formation and the interaction of these plumes with the Nashville urban plume [*Hubler et al.*, 1998; *McNider et al.*, 1998]. The power plant plumes can be identified by increased SO_2 concentrations whereas the urban plume can be detected by elevated CO concentration [*Brock et al.*, 2002]. The very high mean SO_2 concentrations at height of ~900 mb in both Figures 9f and 11f indicate that both periods were strongly influenced by the power plant plumes. This means that on the contrary to the observations at the GSM, the air masses in these two periods over Nashville contained substantial portions of material directly emitted by the power plants. Therefore it is not surprising that the observed aerosol size distributions contained some large particles (radius > 0.5 μm) that may be not sulfate in the two periods as shown in Figure 11. This can explain the systematic underprediction of mass mean radius (Figures 9d and 10d) because the large particles other than sulfate in observations can make a substantial contribution to mass mean radius. This may be the reason that *Von Salzen et al.* [2000] also found their modeled mean mass radii based on sulfate smaller than the observations over Tennessee as well.

4. Spatial Distributions of Microphysical Properties of Aerosols Over the Eastern United States During Summer

[39] One of the major goals of this model is to simulate aerosol microphysical properties over the eastern United States. Since our results were based only on the 40-day simulation from 19 July to 28 August 1995 and even the occurrence of a hurricane (Erin) during the period, it is necessary to consider these extreme meteorological conditions when these results are compared to other model results. Figure 12 shows the horizontal spatial distributions of the 40-day mean sulfate mixing ratios and number concentrations at the lowest model layer over the eastern United States for the base case. As can be seen, the high sulfate mixing ratios are located around the Ohio River valley, whereas the high number concentrations are located over the northeastern coast (New Jersey area) as well as the Ohio River valley. This is generally in agreement with the observations of eastern United States $PM_{2.5}$ and PM_{10} patterns [*Environmental Protection Agency* (*EPA*), 1996], in which the summer peaks (~40 μg m^{-3} for PM_{10} and ~24 μg m^{-3} for $PM_{2.5}$) were determined over the Ohio River valley where sulfate is a major component of PM. As mass mean radii are available over eastern United States in the modeling study of *von Salzen et al.* [2000], it is of interest to compare our results with theirs, although a direct comparison of the results of the two studies might not be

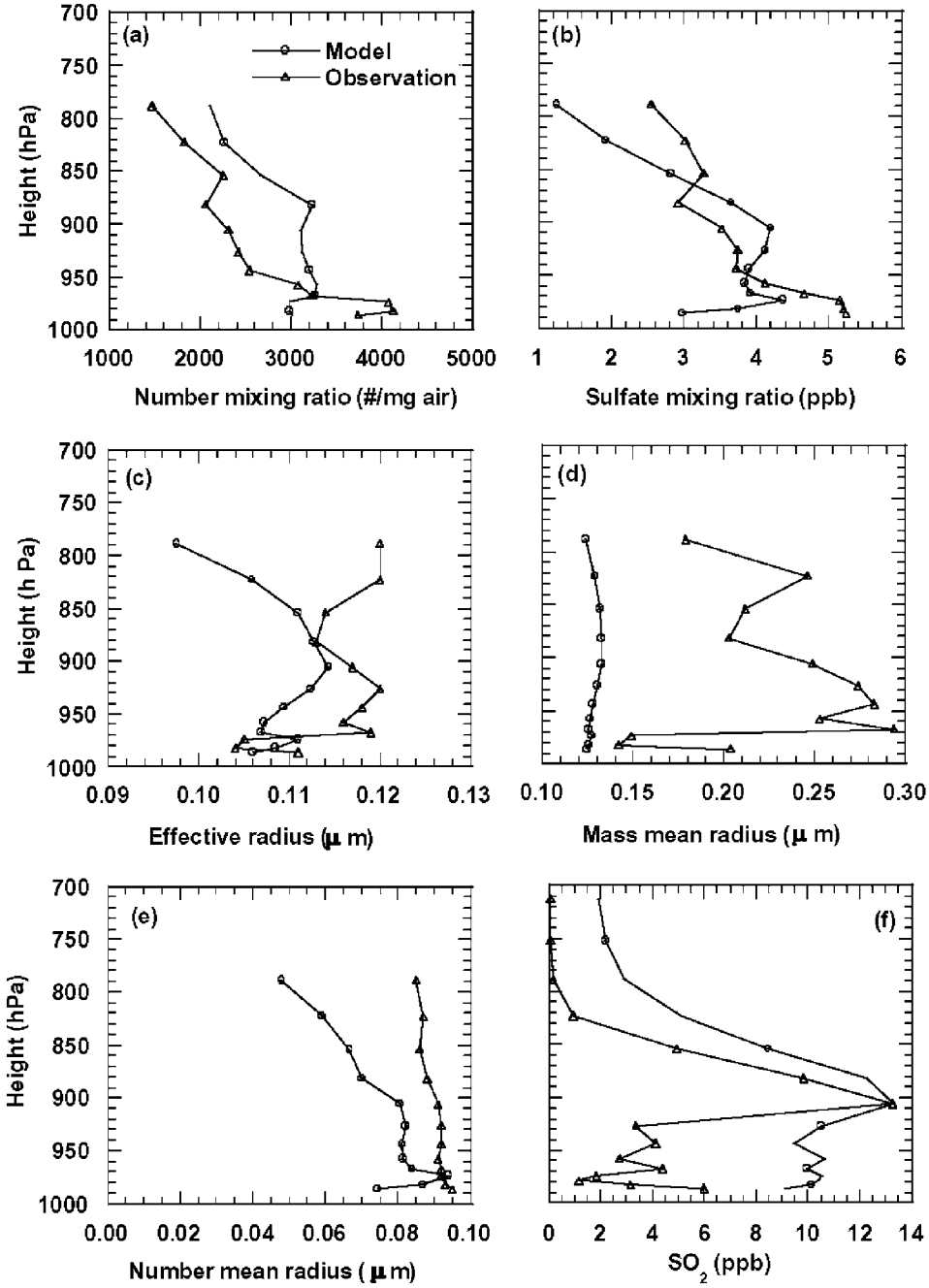

Figure 9. Vertical profiles of modeled and observed (a) number mixing ratios, (b) sulfate mixing ratios, (c) effective radii, (d) mass mean radii, (e) number mean radii, and (f) SO_2 mixing ratios as a function of height (pressure) at Nashville, TN, during period 1 (1400 UT-1800 UT on 19 July 1995). Note that 1 particle mg^{-1} of air corresponds to 0.78 particle cm^{-3} at 1 bar and 273 K.

appropriate because of different years (17–30 July 1995 in this study versus 17–30 July 1994 of *von Salzen et al.* [2000]). The mass mean radius at ambient relative humidity in the present simulation is 0.15 ± 0.013 (one standard deviation) μm, fairly close to but somewhat higher than the mean value obtained by *von Salzen et al.* [2000] (0.11 ± 0.030 μm) for the corresponding cells over the eastern United States. Examination of the spatial distributions of mass mean radius from the two models did not show evidence of strong spatial correlation. The reasons for this are not known: differences in emissions, models, or controlling meteorology.

[40] To better understand the sources and vertical profiles of sulfate properties, we analyzed the sulfate aerosol properties and carried out process analysis at the three specific locations over New Jersey, the Ohio River valley, and the Atlantic Ocean shown in Figure 12a. Figure 13 shows the vertical profiles of mean number concentration, sulfate, SO_2, and H_2SO_4 mixing ratios, and mass mean radii at the three locations. As expected, both mean sulfate mixing

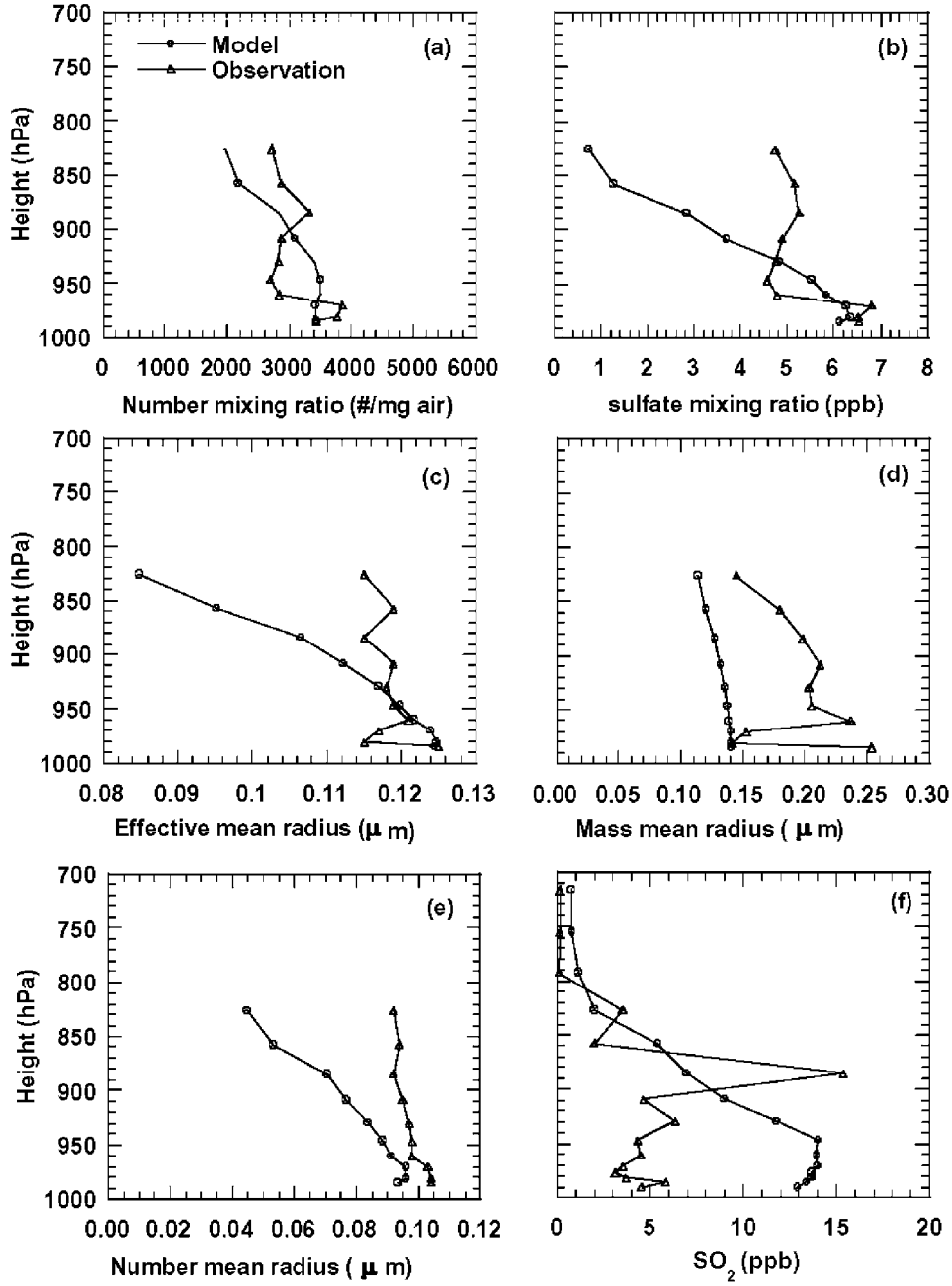

Figure 10. Same as Figure 9 but for the period 2 (1200 UT-1600 UT on 20 July 1995).

ratios and number concentrations over the Ohio River valley were much higher than those over the other two locations below layer 11 (~1.4 km). Somewhat surprisingly, sulfate mixing ratios over the Atlantic Ocean location were greater than those over the New Jersey location below layer 6 (~340 m) whereas the number concentrations over the Atlantic Ocean location were lower at the low model layers. This is consistent with the larger mass mean radii over the Atlantic Ocean location (Figure 13). As expected, both SO_2 and H_2SO_4 vertical profiles were the lowest over the Atlantic Ocean location. Because the number of layers used for emissions was limited to 14 (~2600 m) in the model, the mean number concentrations, sulfate, SO_2, and H_2SO_4 mixing ratios, and mass mean radii are very close for the three locations above layer 15 (Figure 13).

[41] To better understand the contribution of each process to formation of sulfate aerosol, we analyzed the column sulfate amount and number changes, and their budget over the three locations for the 40-day simulation period (Table 2). Seventy-seven percent of total sulfate was located below layer 14 (~2.6 km) over both the New Jersey and Ohio River valley locations whereas only 56% sulfate was located below layer 14 for the Atlantic Ocean location. Aqueous phase reaction of SO_2 is the dominant sulfate source, contributing 70% over both the New Jersey and Ohio River valley locations. This is in agreement with *Roelofs et al.* [2001], who found on the basis of the simulations of 11 global sulfur cycle models that the contributions of aqueous phase oxidation of SO_2 were 59–67% for eastern North America. Over the Atlantic

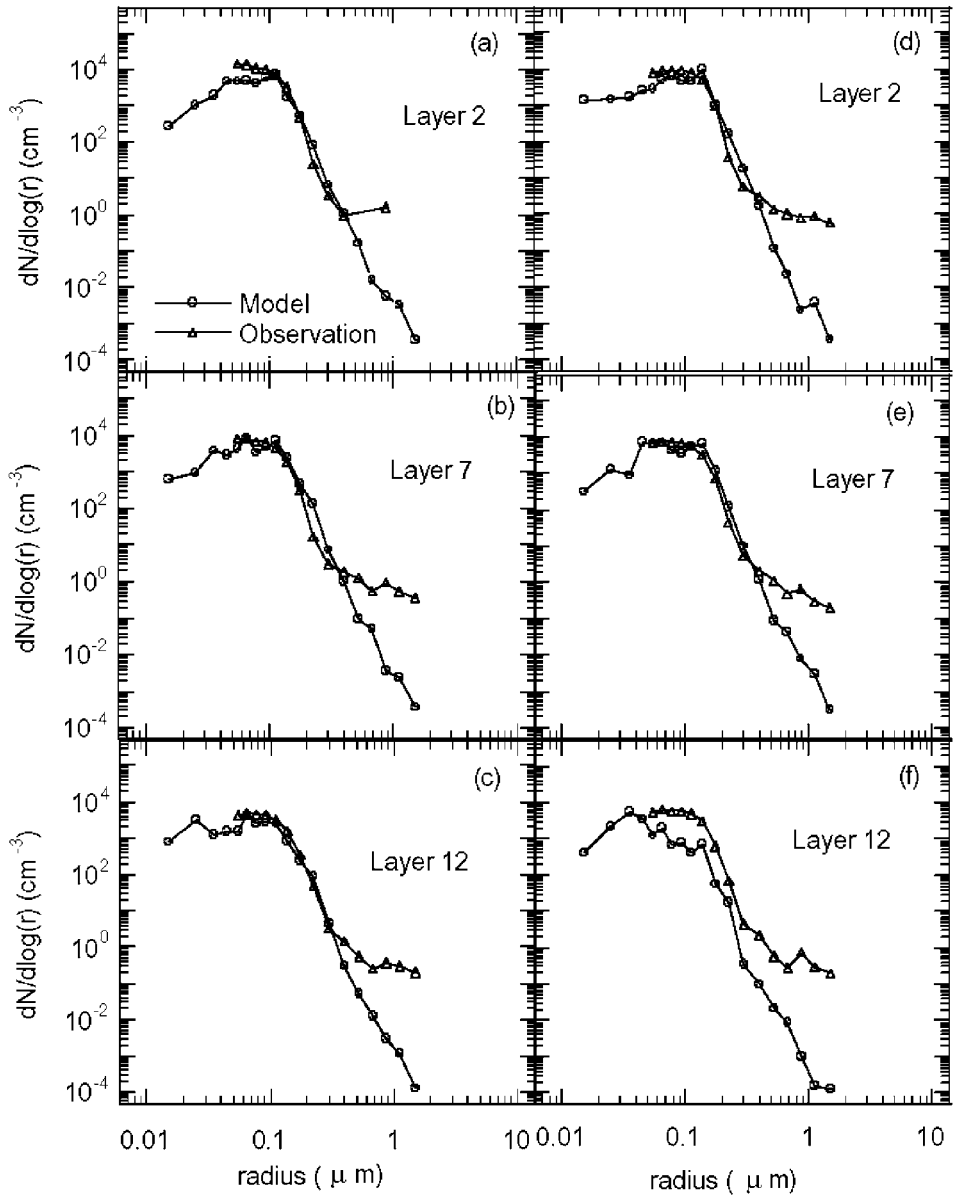

Figure 11. Same as Figure 5 but for layers 2 (∼76 m), 7 (∼480 m), and 12 (∼1750 m) at Nashville, TN, during period 1 (1400 UT-1800 UT on 19 July 1995) (a, b, and c) and period 2 (1200 UT-1600 UT on 20 July 1995) (d, e, and f).

Ocean location, the aqueous reaction of SO_2 contributed 82% of total sulfate source due to the absence of emissions there. The contributions of gas phase reaction through condensation and nucleation to sulfate amount range from 18% over both the Atlantic Ocean and Ohio River valley locations to 17% over New Jersey location. Wet deposition was an important sink over all three locations (Table 2). Wet deposition was the major sink over the southern Atlantic Ocean (98%), whereas it contributed 24 and 33% to the total sink over New Jersey and the Ohio River valley, respectively. These results indicate that the contribution of each process to the sulfate mass fluxes can vary greatly from one area to another. The sulfate mass column amounts (Table 2) were substantially higher than those of *Kasibhatla et al.* [1997a] (∼0.156 mmol m^{-2}) and *Roelofs et al.* [2001] (0.133 mmol m^{-2}) on the basis of the global CTM simulations for eastern North America in summer. However, as our results were for a 40-day period, these results may be not comparable.

[42] In contrast to the sulfate amount, the percentages of total number of particles located below layer 14 (∼2.6 km) were 59, 48, and 14% over the Ohio River valley, New Jersey, and Atlantic Ocean locations, respectively. The major portion of sulfate mass was located below 2.6 km whereas most of the particle number was above 2.6 km except over the Ohio River valley location (Table 2). This is reasonable because the large particles with major mass will exist at the low layers of the atmosphere and small particles with big contribution to total number concentration will exist at the high layers of the atmosphere. As analyzed by *Adams and Seinfeld* [2002], this vertical profile results from higher nucleation rates in the upper troposphere and tropopause

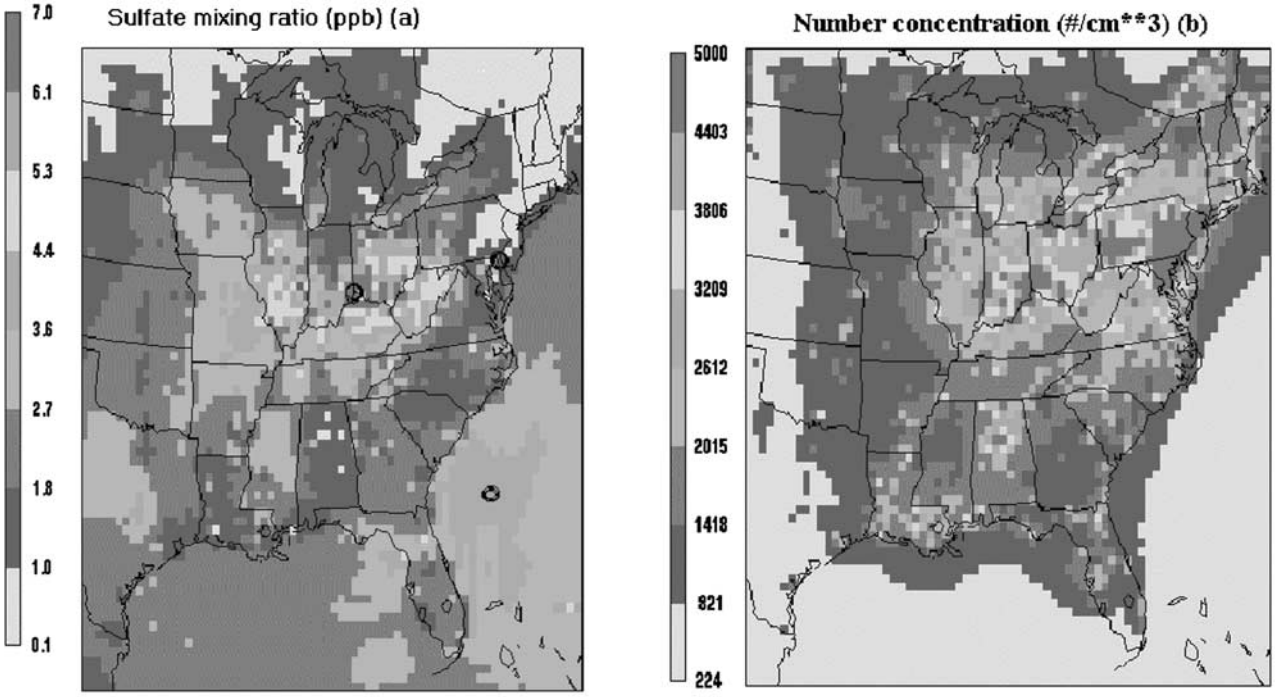

Figure 12. The 40-day average values of the horizontal distributions of (a) mean sulfate mixing ratios (ppb) and (b) number (μ_0, cm^{-3}) concentrations at the lowest model layer. Circles at Ohio River valley, New Jersey, and the Atlantic Ocean east of Georgia in Figure 12a denote the locations selected for budget analysis (see the explanation in text). The middle cells of the surrounding nine cells (3×3) for each area are cell (60,50) (latitude: 39.41°N, longitude: −76.13°W), cell (40,46) (latitude: 38.87°N, longitude: −84.86°W) and cell (60,22) (latitude: 30.31°N, longitude: −77.94°W) for New Jersey area, Ohio River valley, and Atlantic Ocean, respectively. See color version of this figure at back of this issue.

regions, in agreement with the observations of *Schröder et al.* [2002]. Over the Ohio River valley, a substantial portion of number budget was located below 2.6 km (layer 14) due to significant emissions below 2.6 km over the area, which are dominant sources of sulfate number concentration as analyzed below. Direct emissions were the dominant sources of particle number over both the New Jersey (99%) and Ohio River valley (96%) locations, whereas nucleation was the only source of particle number at the Atlantic Ocean location as listed in Table 2. As expected, coagulation was the dominant sink of particle number for all locations. Note that at the Ohio River valley and New Jersey locations total production of both sulfate amount and number substantially exceeds removal, whereas at the Atlantic Ocean location total removal exceeds production (Table 2). This indicates that the transport moved out substantial portions of the sulfate mass and number from the Ohio River valley and New Jersey locations, but there was a net import of sulfate mass and number into the Atlantic Ocean location. This is due to the fact that there was substantial emission at the Ohio River valley and New Jersey locations, as well as substantial sulfate formation by reaction, whereas at the Atlantic Ocean location there was no emission and much less reaction.

[43] The lifetime of sulfate number is much shorter than sulfate amount because of the strong removal process of coagulation for the sulfate number (Table 2). For the three studied locations, the lifetimes of both sulfate amount and number over the Atlantic Ocean location (8.05 days for amount and 1.70 days for number) were much longer than those over the New Jersey location (4.97 days for amount and 0.38 days for number) and Ohio River valley location (2.56 days for mass and 0.17 days for number). The smaller wet removal and coagulation rates over the Atlantic Ocean location lead to longer lifetimes for sulfate amount and number, respectively, as shown in Table 2. The longer lifetime of sulfate amount and number over the Atlantic Ocean may be another reason for the particles to become bigger than other locations (Figure 13). In the results of *Roelofs et al.* [2001], *Kasibhatla et al.* [1997a, 1997b], and *Chin et al.* [2000], the lifetimes of sulfate amount for eastern North America were 2.0–5.4, 2.7, and 3.4 days, respectively. Our results seem consistent with these results, especially over the New Jersey and Ohio River valley locations.

5. Summary and Conclusions

[44] A six-moment aerosol microphysical module (6M) has been implemented in a regional 3-D air quality model (MAQSIP) and applied to sulfate aerosol in the eastern United States for 40-day simulation of July to August 1995. The model successfully captured the observed size distribution in the accumulation mode (radius 0.1–0.5 μm), in which the sulfate is predominately located, on the basis of the size distributions retrieved from the modeled six moments at the GSM during the SEAVS. These results demonstrate the utility as well as the efficiency of moment-based models. A 1-day simulation needs ~8 hours computer

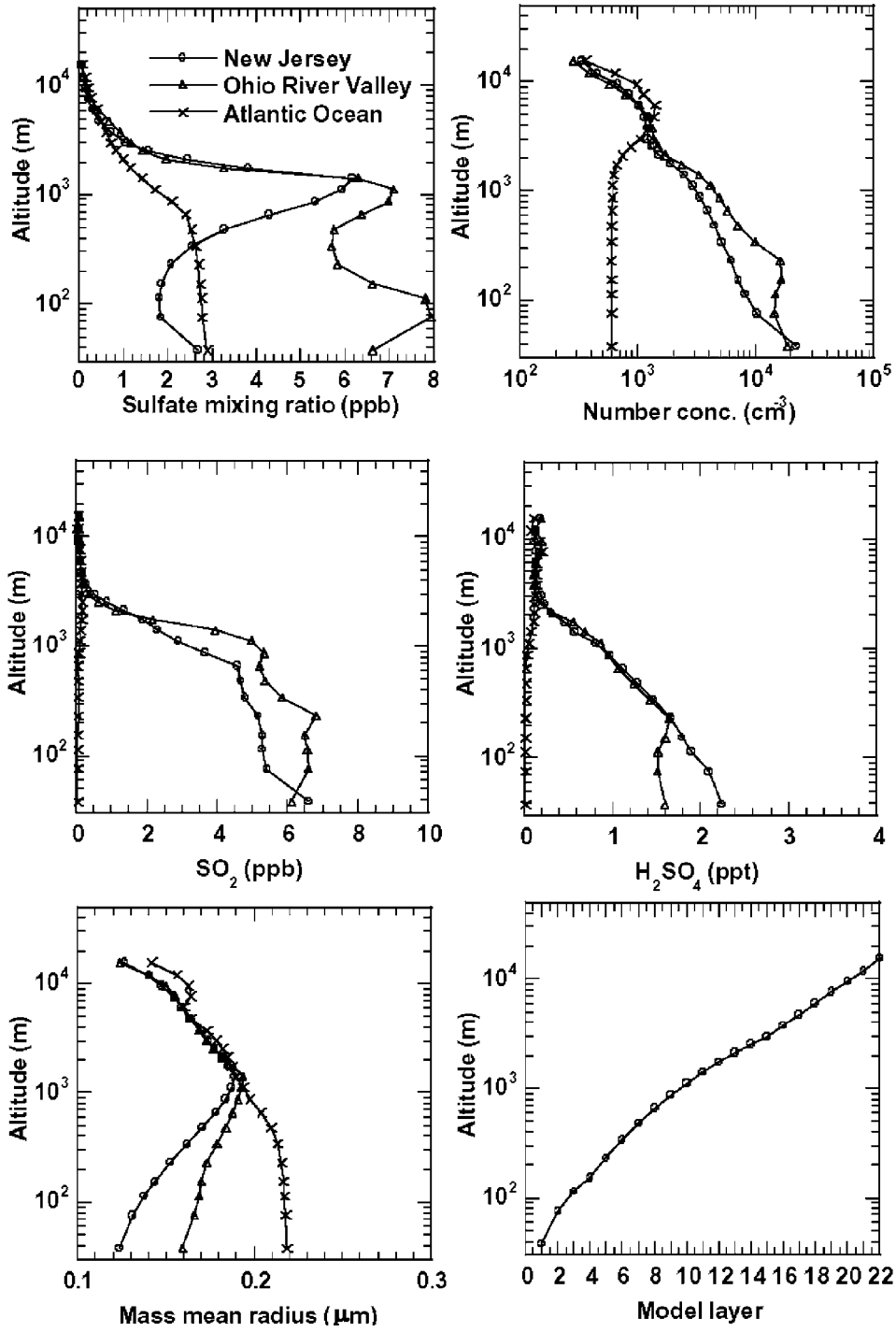

Figure 13. The mean vertical profiles of sulfate mass, SO_2, and H_2SO_4 mixing ratios, number concentration, and mass mean radii over the three locations (New Jersey, Ohio River valley, and Atlantic Ocean) during the 40-day simulation period. Height for each layer is also shown in the last panel.

time at a single-processor Sun (ULTRA 60) station. However, the model did not predict some of the moments well, especially the higher moments during dust events. Over the eastern United States, the domain average of modeled SO_4^{2-} mixing ratios was 13% lower than the observations, with about 50% of the observations simulated to within a factor of 2. One of the reasons for this underestimation of sulfate mixing ratios is thought to be overprediction of sulfate wet deposition. Reduction of the fraction of sulfate taken into cloud water from 100 to 50% does not improve the model performance spatially over the eastern United States. The model systematically overestimated the observed SO_2 mixing ratios, by a factor of 2.4, on an average.

[45] The sensitivity test with doubled condensation rate suggests that most of the aerosol surface area, determined mainly by the accumulation mode, is well represented by the modeled sulfate. This is supported by the results that the model reproduced the effective radii better than other size

Table 2. Column Integral of Change and Column Amount in Sulfate and Number Concentrations by Each Process at Three Locations Over New Jersey, Ohio Valley, and Atlantic Ocean During the 40-Day Simulation Period[a]

	Ohio River Valley	New Jersey	Atlantic Ocean
Sulfate Amount Column Change ($mmol\ m^{-2}d^{-1}$)			
Aqueous phase reaction	0.56	0.33	0.028
Emission	0.15	0.059	0
Nucleation	2.12×10^{-5}	0.45×10^{-5}	0.19×10^{-5}
Condensation	0.097	0.080	0.0055
Total production	0.81	0.47	0.034
Wet deposition	−0.26	−0.11	−0.04
Dry deposition	-9.32×10^{-4}	-6.01×10^{-4}	-6.19×10^{-4}
Total removal	−0.26	−0.11	−0.04
Sulfate Column Amount ($mmol\ m^{-2}$)			
Total	0.67	0.54	0.33
Below layer 14 (∼2.6 km)	0.52	0.42	0.19
In layer 1 (∼38 m)	1.12×10^{-2}	0.46×10^{-2}	0.49×10^{-2}
Lifetime, day	2.56	4.97	8.05
Number Column Change ($10^8 cm^{-2}d^{-1}$)			
Emission	136.0	55.1	0
Nucleation	6.15	0.79	0.19
Total production	142.2	55.9	0.19
Wet deposition	−3.9	−0.95	−0.62
Coagulation	−114	−42.7	−6.94
Dry deposition	−0.56	−1.0	-6.0×10^{-3}
Total removal	−118.4	−44.6	−7.56
Number Column Amount ($10^8 cm^{-2}$)			
Total	20.3	17.1	12.9
Below layer 14 (∼2.6 km)	11.9	8.18	1.74
In layer 1 (∼38 m)	0.07	0.08	0.002
Lifetime, day	0.17	0.38	1.70

[a]Lifetime is defined as the ratio of column amount to the total loss rate excluding transport.

parameters. Over Nashville during the SOS, the model closely reproduced the observed size distributions between 0.10 and 0.45 μm (dry radius), and the observed and modeled sulfate mass concentrations are close as well. However, the model seriously underpredicted the observed high moments of total aerosol size distributions at the GSM during the periods when the site was influenced by the dust or the air mass transported from the Ohio River valley. Comparison of the observed and retrieved size distributions on the basis of the modeled six moments indicates that the model underpredicts the observed large particles (radius > 0.5 μm, coarse mode) and small particles (radius < 0.1 μm, nucleation mode) at the GSM, and underpredicts the observed large particles over Nashville as well. In situ chemical analyses indicates that other aerosol components such as dust and organics might make a substantial contribution to the observed particles in these two size ranges. Errors in the representation of sulfate nucleation or primary sulfate emissions might also cause these discrepancies, especially for the nucleation mode.

[46] On the basis of the simulation of sulfate aerosols, it was found that the highest sulfate mass concentrations were located around the Ohio River valley whereas the highest number concentrations were located over the northeastern coast (New Jersey area) and Ohio River valley. On the basis of column integral change and burden analysis of sulfate amount and number over the three locations, it was found that the contribution of each process varied considerably from one location to another. The major portion of sulfate mass was located below 2.6 km and most of sulfate number located above 2.6 km except over Ohio River valley where there was a major low-altitude input from emissions.

[47] There are uncertainties in both quantitatively describing the aerosol dynamics and microphysics, and other atmospheric processes such as advection and diffusion represented in the model. Uncertainties in nucleation processes and rates are major limiting factors in modeling particle number and thus the modeling of other aerosol properties, for which accurate knowledge of aerosol number is required. In light of these uncertainties, the performance of our 6M moment-based module in the regional model can be considered to successfully represent aerosol evolution and properties. On the other hand, as shown in comparisons with observations over GSM and Nashville, TN, accurate representation of properties of the whole aerosol obviously must include other important aerosol constituents such as dust and organics, especially for the eastern United States.

Appendix A: Calculations of Weighting Function for Distributing the Precipitation Rates to Each Layer

[48] As mixing ratios of water vapor (q_v), cloud water q_c (ice, q_i), rainwater q_r (snow, q_s) mixing ratios (g kg^{-1}) and meteorological parameters such as wind speed are generated by the MM5, the weighting function for calculating the precipitation rates at each resolved cloud layer can be based on this available information. The steps to get the weighting function according to the equation for rainwater mixing ratios in the MM5 [*Grell et al.*, 1994] are as follows:

A1. Step 1

[49] The rates at which cloud water is converted into precipitation through autoconversion (P_{RC}) and accretion (P_{RA}) processes, and the evaporation of rain (P_{RE}) are determined as follows [*Grell et al.*, 1994]:

$$P_{RC} = k_1(q_c - q_{crit}), \tag{A1}$$

$$P_{RA} = \frac{1}{4}\pi a q_c E N_0 \frac{\Gamma(3+b)}{\lambda^{3+b}}, \tag{A2}$$

$$P_{RE} = \frac{2\pi N_0(S-1)}{A+B}\left[\frac{f_1}{\lambda^2} + f_2\left(\frac{a\rho}{\mu}\right)^{1/2} S_c^{1/3}\frac{\Gamma(5/2+b/2)}{\lambda^{5/2+b/2}}\right], \tag{A3}$$

$$\lambda = \left(\frac{\pi N_0 \rho_w}{\rho q_r}\right)^{1/4},$$

$$A = \frac{L_w^2 \rho}{K_a R_v T^2},$$

$$B = \frac{1}{q_{sw}\chi},$$

$$S_c = \frac{\mu}{\rho\chi},$$

where the parameters (N_0, a, b) of Marshall-Palmer size distributions for rain are: $N_0 = 8 \times 10^6$ m^{-4}, $a = 842$ m^{1-b} s^{-1}, $b = 0.8$, $f_1 = 0.78$, $f_2 = 0.32$, Γ is the gamma function, μ is the dynamic viscosity of air, χ is diffusivity of vapor in air (m^2 s^{-1}), ρ and ρ_w are the densities of air and rain, respectively, $q_{\text{crit}} = 0.5$ g kg^{-1}, and $k_1 = 10^{-3}$ s^{-1}, E is the collection efficiency (1 for rain, 0.1 for snow), L_w is the latent heat of evaporation, K_a is the thermal conductivity of air, R_v is the gas constant for water vapor (461.5 J kg^{-1} K^{-1}), T is the temperature (K), q_{sw} is saturated vapor mixing ratio with respect to water, and S is relative humidity.

A2. Step 2

[50] The advection term in the equation for rainwater mixing ratio is estimated on the basis of rainwater mixing ratios and wind speeds at two cells adjacent to the cell, e.g., for x direction,

$$\frac{\Delta(u(i)q_r(i))}{\Delta x} = \frac{u(i+1)q_r(i+1) - u(i-1)q_r(i-1)}{2\Delta x}, \quad \text{(A4)}$$

where u is wind speed for x direction and Δx is grid distance of the cell.

A3. Step 3

[51] By ignoring the divergence and diffusion terms that are small in the equation for rainwater mixing ratio, we estimate the rainfall term in the equation for each cell on the basis of output of cloud water mixing ratios and rainwater mixing ratios for each hour from MM5 as follows:

$$\Delta R_N \cong [(P_{\text{RE}} + P_{\text{RC}} + P_{\text{RA}})\Delta t - \Delta q_r - \text{advection} \times \Delta t], \quad \text{(A5)}$$

where Δt is the time interval for model output (1 hour).

[52] As MM5 does not output the production terms in equation (A5), we would have to rerun the MM5 and force it to output the instantaneous values for these terms if we want to evaluate each term in equation (A5). This is beyond the scope of this paper. However, the MM5 output surface precipitation amount is computed using these production terms in the model. Therefore we can compare the MM5 predicted surface precipitation to that estimated from equation (A5). We found that the correlation between them was very high (correlation coefficient was 0.888 for 35-day data (number of point is 5328)) for our studied region. This indicates that as a postprocessing tool, equation (A5) can be used to estimate the rainwater flux at all layers. In this study, we use the estimated rainfall by equation (A5) as weighting functions to distribute the rainfall output from MM5 vertically to each layer.

Appendix B: In-Cloud and Below-Cloud Scavenging of SO_2, H_2SO_4, and Sulfate Aerosols

[53] In this study, both rainout (in-cloud scavenging) and washout (below-cloud scavenging) are treated as first-order loss and simultaneous processes without operator splitting. The first-order loss rate constant (K_r) for rainout is

$$K_r = \frac{R_r/(\Delta z)}{W_c}, \quad \text{(B1)}$$

where $R_r$is the precipitation rate for the whole cell (kg m^{-2} s^{-1}), Δz is the layer thickness (m), and W_c is a liquid water content of cloud for the whole cell (kg m^{-3}). For washout the rate constant (K_w) is

$$K_w = \Lambda(r)R_a/f_c, \quad \text{(B2)}$$

where $\Lambda(r)$ is a washout coefficient (mm^{-1}) normalized to the precipitation rate [*Dana and Hales*, 1976] and f_c is the cloud cover fraction for the cell. For gaseous species $\Lambda(r)$ is assumed to be 0.1 mm^{-1}. For aerosols, $\Lambda(r)$ depending on retrieved r_g and σ_g was computed on the basis of calculations of Dana and Hales for mass washout coefficients [Figure 2 of *Dana and Hales*, 1976] with the fourth-order polynomial equation. The lognormal parameters N, r_g, and σ_g are obtained algebraically from any three of the six moments: μ_0, μ_1, and μ_3 are used here. R_a is the total precipitation rate integrated over all model layers above the whole cell currently treated (mm s^{-1}).

[54] SO_2 is partitioned according to Henry's Law between the gas phase, the cloud water, and the rainwater from above that will pass through the cell during the time step. First, we partition the SO_2 between the gas phase and the "total aqueous phase" consisting of the cloud water in the present cell plus the rainwater passing through the cell from all layers above the cell. The fraction of SO_2 in the aqueous phase is

$$F_{\text{aq}} = \frac{K_{\text{H}}(W_c + W_r)RT/\rho_{\text{H}_2\text{O}}}{1 + K_{\text{H}}(W_c + W_r)RT/\rho_{\text{H}_2\text{O}}}, \quad \text{(B3)}$$

where K_{H} is the Henry's Law constant for SO_2 (M atm^{-1}), R is the ideal gas law constant, T is the temperature (K), ρ_{H_2}O is the density of water = 1000 kg m^{-3}. The dependence of K_{H} on pH is considered with the method of *Schwartz* [1986] on the assumption that pH is 4.5. The rainwater (W_r, kg m^{-3}) is

$$W_r = \frac{R_a \Delta t}{\Delta z}. \quad \text{(B4)}$$

So the fraction of SO_2 in the cloud water (F_{cw}) is:

$$F_{\text{cw}} = \frac{K_{\text{H}}(W_c)RT/\rho_{\text{H}_2\text{O}}}{1 + K_{\text{H}}(W_c + W_r)RT/\rho_{\text{H}_2\text{O}}} \quad \text{(B5)}$$

and the fraction of SO_2 in the rainwater (F_{rw}) is:

$$F_{\text{rw}} = \frac{K_{\text{H}}(W_r)RT/\rho_{\text{H}_2\text{O}}}{1 + K_{\text{H}}(W_c + W_r)RT/\rho_{\text{H}_2\text{O}}}. \quad \text{(B6)}$$

The total SO_2 concentration at time t, $[SO_2]_{\text{tot}}(t)$, in the grid cell is partitioned as

$$[\text{SO}_2]_{\text{cw}}(t) = F_{\text{cw}}[\text{SO}_2]_{\text{tot}}(t),$$

$$[\text{SO}_2]_{\text{rw}}(t) = F_{\text{rw}}[\text{SO}_2]_{\text{tot}}(t),$$

$$[\text{SO}_2]_g(t) = (1 - F_{\text{cw}} - F_{\text{rw}})[\text{SO}_2]_{\text{tot}}(t),$$

where cw, rw, and g represent cloud water, rainwater, and gaseous phase, respectively. These concentrations are then updated as follows:For rainout we have

$$[SO_2]_{cw}(t+\Delta t) = [SO_2]_{cw}(t)\exp(-K_R\Delta t). \quad \text{(B7)}$$

For washout, the treatment depends on whether the process is limited by mass transfer

$$[SO_2]_{rw}(t+\Delta t) = [SO_2]_{rw}(t)\exp(-K_w\Delta t)$$
$$\text{if } F_{rw} > 1-\exp(-K_w\Delta t)$$
$$\text{with } \Lambda(r) = 0.1\,\text{mm}^{-1}$$

or Henry's Law equilibrium:

$$[SO_2]_{rw}(t+\Delta t) = [SO_2]_{rw}(t)\exp(-K_w\Delta t)$$
$$\text{if } F_{rw} < 1-\exp(-K_w\Delta t) \quad \text{(B8)}$$
$$\text{with } \Lambda(r) = 0.1\,\text{mm}^{-1}$$

The gas phase portion remains unchanged by these processes as follows:

$$[SO_2]_g(t+\Delta t) = [SO_2]_g(t).$$

The updated total SO_2 concentration in cloudy portion of the cell is

$$[SO_2]_{cld}(t+\Delta t) = [SO_2]_{cw}(t+\Delta t) + [SO_2]_{rw}(t+\Delta t) + [SO_2]_g(t+\Delta t).$$

If the cloud cover fraction (f_c) is less than unity, the updated mean SO_2 in the whole cell is

$$[SO_2](t+\Delta t) = f_c[SO_2]_{cld}(t+\Delta t) + (1-f_c)[SO_2]_{clr}(t+\Delta t),$$

where the updated SO_2 concentration in clear-sky portion of the cell $[SO_2]_{clr}(t+\Delta t) = [SO_2](t)$ since at this point in the model integration clear-sky processes are not currently being treated. H_2SO_4 is assumed to be completely in the aqueous phase, and partitioned between the cloud water and rainwater according to their relative amounts:

$$[H_2SO_4]_{cw}(t) = [H_2SO_4](t)\frac{W_c}{W_c+W_r}$$

$$[H_2SO_4]_{rw}(t) = [H_2SO_4](t)\frac{W_r}{W_c+W_r}$$

and the updating is

$$[H_2SO_4]_{cw}(t+\Delta t) = [H_2SO_4]_{cw}(t)\exp(-K_r\Delta t)$$

$$[H_2SO_4]_{rw}(t+\Delta t) = [H_2SO_4]_{rw}(t)\exp(-K_w\Delta t)$$

and the updated total H_2SO_4 concentration in cloudy portion of the cell is

$$[H_2SO_4]_{cld}(t+\Delta t) = [H_2SO_4]_{cw}(t+\Delta t) + [H_2SO_4]_{rw}(t+\Delta t).$$

If the cloud cover fraction is less than unity, the updated mean H_2SO_2 in the whole cell is

$$[H_2SO_4](t+\Delta t) = f_c[H_2SO_4]_{cld}(t+\Delta t) + (1-f_c)[H_2SO_4]_{clr}(t+\Delta t),$$

where

$$[H_2SO_4]_{clr}(t+\Delta t) = [H_2SO_4](t).$$

[55] Sulfate aerosol is assumed to be completely in the aqueous phase, and partitioned between the cloud water and rainwater according to their relative amounts. The number concentration of the aerosol (μ_0) is partitioned as

$$[\mu_0]_{cw}(t) = [\mu_0](t)\frac{W_c}{W_c+W_r}$$

$$[\mu_0]_{rw}(t) = [\mu_0](t)\frac{W_r}{W_c+W_r}$$

and the updating is

$$[\mu_0]_{cw}(t+\Delta t) = [\mu_0]_{cw}(t)\exp(-K_r\Delta t)$$

$$[\mu_0]_{rw}(t+\Delta t) = [\mu_0]_{rw}(t)\exp(-K_w\Delta t)$$

and the updated mean aerosol number concentration in the cloud fraction of the cell is

$$[\mu_0]_{cld}(t+\Delta t) = [\mu_0]_{cw}(t+\Delta t) + [\mu_0]_{rw}(t+\Delta t).$$

If the cloud cover fraction is less than unity, the updated mean aerosol number concentration in the whole cell is

$$[\mu_0](t+\Delta t) = f_c[\mu_0]_{cld}(t+\Delta t) + (1-f_c)[\mu_0]_{clr}(t+\Delta t).$$

[56] As the removal must be done after completing the microphysical processes, we save the factor:

$$f_{\text{fract}} = \frac{[\mu_0]_{cld}(t+\Delta t)}{[\mu_0](t)}$$

to represent the fraction of the aerosol remaining after rainout and washout in the cloudy portion of cell. Note that this fraction of the aerosol was also applied to all six moments because the moments of a PDF are not mathematically independent quantities as analyzed in section 2.2.

[57] **Acknowledgments.** We thank S. Kreidenweis, W. Malm, B. Schichtel, J. Sisler, J. Hand, and R. Ames for providing IMPROVE and SEAVS data sets, R. Larson for NADP data, L.I. Kleinman for the SOS data set, and K. von Salzen for the results of the NARCM. We also thank U. Shankar and R. Mathur for supplying the MAQSIP model. We thank two

anonymous referees for their helpful comments on the manuscript. Work done at Duke was supported by grant NA76GP0350 from NOAA Office of Global Programs, and subcontract G-35-W62-G2 from Georgia Institute of Technology (principal grant R 826372-01-0 from EPA). Work done at BNL was supported in part by NASA through interagency agreement W-18,429 as part of its interdisciplinary program on tropospheric aerosols, and in part by the Environmental Sciences Division of the U.S. Department of Energy (DOE) as part of the Atmospheric Chemistry Program, and was performed under the auspices of DOE under contract DE-AC02-98CH10886.

References

Abdul-Razzak, H., S. J. Ghan, and C. Rivera-Carpio, A parameterization of aerosol activation: 1. Single aerosol type, *J. Geophys. Res.*, *103*, 6123–6131, 1998.

Adams, P. J., and J. H. Seinfeld, Predicting global aerosol size distributions in general circulation models, *J. Geophys. Res.*, *107*(D19), 4370, doi:10.1029/2001JD001010, 2002.

Ames, R. B., J. L. Hand, S. M. Kreidenweis, D. E. Day, and W. C. Malm, Optical measurements of aerosol size distributions in Great Smoky Mountains National Park: Dry aerosol characterization, *J. Air Waste Manage. Assoc.*, *50*, 665–676, 2000.

Andrews, E., P. Saxena, S. Musarra, L. M. Hildemann, P. Koutrakis, P. H. McMurry, I. Olmez, and W. H. White, Concentration and composition of atmospheric aerosols from the 1995 SEAVS experiment and a review of the closure between chemical and gravimetric measurements, *J. Air Waste Manage. Assoc.*, *50*, 648–664, 2000.

Barrett, J. C., and N. A. Webb, A comparison of some approximate methods for solving the aerosol general dynamic equation, *J. Aerosol Sci.*, *29*, 31–39, 1998.

Barth, M. C., P. J. Rasch, J. T. Kiehl, C. M. Benkovitz, and S. E. Schwartz, Sulfur chemistry in the National Center for Atmospheric Research Community Climate Model: Description, evaluation, features, and sensitivity to aqueous chemistry, *J. Geophys. Res.*, *105*, 1387–1415, 2000.

Benkovitz, C. M., and S. E. Schwartz, Evaluation of modeled sulfate and SO_2 over North America and Europe for four seasonal months in 1986–1987, *J. Geophys. Res.*, *102*, 25,305–25,338, 1997.

Binkowski, F. S., and U. Shankar, The regional particulate model: 1. Model description and preliminary results, *J. Geophys. Res.*, *100*, 26,191–26,209, 1995.

Birmili, W., and A. Wiedensohler, The influence of meteorological parameters on ultrafine particle production at a continental site, *J. Aerosol Sci.*, *29*, S1015–S1016, 1998.

Brock, C. A., et al., Particle growth in the plumes of coal-fired power plants, *J. Geophys. Res.*, *107*(D12), 4155, doi:10.1029/2001JD001062, 2002.

Byun, D. W., and J. K. S. Ching, Science algorithms of the EPA Models-3 community multiscale air quality (CMAQ) modeling system, *USA EPA/600/R-99/030*, U.S. Environ. Prot. Agency, U.S. Govt. Print. Off., Washington, D. C., 1999.

Chang, J. S., R. A. Brost, I. S. A. Isaksen, S. Madronich, P. Middleton, W. R. Stockwell, and C. J. Walcek, A three-dimensional Eulerian acid deposition model: Physical concepts and formation, *J. Geophys. Res.*, *92*, 14,681–14,700, 1987.

Chang, J. S., et al., The regional acid deposition model and engineering model, in *National Acid Precipitation Program, Acidic Deposition: State of Science and Technology*, vol. 1, *NAPAP SOS/T Rep. 4*, Natl. Acid Precip. Program, Washington, D. C., 1990.

Chin, M., D. L. Savoie, B. J. Huebert, A. R. Bandy, D. C. Thornton, T. S. Bates, P. K. Quinn, E. S. Saltzman, and W. J. Bruyn, Atmospheric sulfur cycle simulated in the global model GOCART: Comparison with field observations and regional budgets, *J. Geophys. Res.*, *105*, 24,689–24,712, 2000.

Dana, M. T., and J. M. Hales, Statistical aspects of the washout of polydispers aerosols, *Atmos. Environ.*, *10*, 45–50, 1976.

Daum, P. H., T. J. Kelly, S. E. Schwartz, and L. Newman, Measurements of the chemical composition of stratiform clouds, *Atmos. Environ.*, *18*, 2671–2684, 1984a.

Daum, P. H., S. E. Schwartz, and L. Newman, Acidic and related constituents in liquid water stratiform clouds, *J. Geophys. Res.*, *89*, 1447–1458, 1984b.

DeMore, W. B., S. P. Sander, D. M. Golden, R. F. Hampson, M. J. Kurlo, C. J. Howard, A. R. Ravishankara, C. E. Kolb, and M. J. Molina, Chemical kinetics and photochemical data for use in stratospheric modeling, *JPL Publ.*, 92–120, 1992.

Dennis, R. L., J. N. McHenry, W. R. Barchet, F. S. Binkowski, and D. W. Byun, Correcting RADM's sulfate underprediction: Discovery and correction of model errors and testing the corrections through comparisons against field data, *Atmos. Environ., Part A*, *26*, 975–997, 1993.

Environmental Protection Agency (EPA), Air quality criteria for particular matter, *EPA/600/P-95/001aF*, 1996.

Feller, W., *An Introduction to Probability Theory and Its Applications*, vol. 2, 155 pp., John Wiley, New York, 1971.

Fitzgerald, J. W., W. A. Hoppel, and F. Gelbard, A one-dimensional sectional model to simulate multicomponent aerosol dynamics in the marine boundary layer: 1. Model description, *J. Geophys. Res.*, *103*, 16,085–16,102, 1998.

Fuchs, N. A., *The Mechanics of Aerosols*, translated by R. E. Daisley and M. Fuchs, Pergamon, New York, 1964.

Gery, M. W., G. Z. Whitten, J. P. Killus, and M. C. Dodge, A photochemical kinetics mechanism for urban and regional scale computer modeling, *J. Geophys. Res.*, *94*, 12,925–12,956, 1989.

Ghan, S. J, R. C. Easter, E. G. Chapman, H. Abdul-Razzak, Y. Zhang, L. R. Leung, N. S. Laulainen, R. D. Saylor, and R. A. Zaveri, A physically based estimate of radiative forcing by anthropogenic sulfate aerosol, *J. Geophys. Res.*, *106*, 5279–5293, 2001.

Giorgi, F., A particle dry-deposition parameterization scheme for use in tracer transport models, *J. Geophys. Res.*, *91*, 9794–9806, 1986.

Grell, G. A., J. Dudhia, and D. R. Stauffer, A description of the Fifth-Generation Penn State/NCAR Mesoscale Model (MM5), *Rep. NCAR/TN-389+STR*, 138 pp., Nat. Cent. for Atmos. Res., Boulder, Colo., 1994.

Hegg, D. A., J. Livingston, P. V. Hobbs, T. Novakov, and P. Russell, Chemical apportionment of aerosol column optical depth off the mid-Atlantic coast of the United States, *J. Geophys. Res.*, *102*, 25,297–25,303, 1997.

Holland, D. M., P. P. Principe, and J. E. Sickles II, Trends in atmospheric sulfur and nitrogen species in the eastern United States for 1989–1995, *Atmos. Environ.*, *33*, 37–49, 1999.

Houyoux, M. R., J. M. Vukovich, C. J. Coats Jr., N. M. Wheeler, and P. S. Kasibhatla, Emission inventory development and processing for the seasonal model for regional air quality (SMRAQ) project, *J. Geophys. Res.*, *105*, 9079–9090, 2000.

Hubler, G., et al., An overview of the airborne activities during the Southern Oxidants Study (SOS) 1995 Nashville/Middle Tennessee Ozone Study, *J. Geophys. Res.*, *103*, 22,245–22,259, 1998.

Husar, R. B., D. E. Patterson, J. D. Husar, N. V. Gillani, and W. E. Wilson Jr., Sulfur budget of a power plant plume, *Atmos. Environ.*, *12*, 549–568, 1978.

Jacobson, M. Z., Analysis of aerosol interactions with numerical techniques for solving coagulation, nucleation, condensation, dissolution, and reversible chemistry among multiple size distributions, *J. Geophys. Res.*, *107*(D19), 4366, doi:10.1029/2001JD002044, 2002.

Jacobson, M. Z., R. P. Turco, E. J. Jensen, and O. B. Toon, Modeling coagulation among particles of different composition and size, *Atmos. Environ.*, *28*, 1327–1338, 1994.

Jaecker-Voirol, A., and P. Mirabel, Heteromolecular nucleation in the sulfuric acid-water system, *Atmos. Environ.*, *23*, 2053–2057, 1989.

Kasibhatla, P., and W. L. Chameides, Seasonal modeling of regional ozone pollution in the eastern United States, *Geophys. Res. Lett.*, *27*, 1415–1418, 2000.

Kasibhatla, P., W. L. Chameides, and S. S. John, A three-dimensional global model investigation of seasonal variations in the atmospheric burden of anthropogenic sulfate aerosols, *J. Geophys. Res.*, *102*, 3737–3759, 1997a.

Kasibhatla, P., W. L. Chameides, B. Duncan, M. Houyoux, C. Jang, R. Mathur, T. Odman, and A. Xiu, Impact of inert organic nitrate formation on ground-level ozone in a regional air quality model using the carbon bond mechanism 4, *Geophys. Res. Lett.*, *24*, 3205–3208, 1997b.

Kavouras, I. G., N. Mihalopoulos, and E. G. Stephanou, Formation of atmospheric particles from organic acids produced by forests, *Nature*, *395*, 683–686, 1998.

Koch, D., D. Jacob, I. Tegen, D. Rind, and M. Chin, Tropospheric sulfate simulation and sulfate direct radiative forcing in the Goddard Institute for Space Studies general circulation model, *J. Geophys. Res.*, *104*, 23,799–23,822, 1999.

Kreidenweis, S. M., J. E. Penner, F. Yin, and J. H. Seinfeld, The effects of dimethylsulfide upon marine aerosol concentrations, *Atmos. Environ.*, *25*, 2501–2511, 1991.

Kulmala, M., A. Toivonen, J. M. Makela, and A. Laaksonen, Analysis of the growth of nucleation mode particles observed in Boreal forest, *Tellus, Ser. B*, *50*, 449–462, 1998.

Langner, J., and H. Rodhe, A global three-dimensional model of the tropospheric sulfur cycle, *J. Atmos. Chem.*, *13*, 225–263, 1991.

Lynch, J. A., J. W. Grimm, and V. C. Bowersox, Trends in precipitation chemistry in the United States, a national perspective, 1980–1992, *Atmos. Environ.*, *29*, 1231–1246, 1995.

McGraw, R., Description of aerosol dynamics by the quadrature method of moments, *Aerosol Sci. Technol.*, *27*, 255–265, 1997.

McGraw, R., and J. H. Saunders, A condensation feedback mechanism for oscillatory nucleation and growth, *Aerosol Sci. Technol.*, *3*, 367–380, 1984.

McGraw, R., and D. L. Wright, Chemically resolved aerosol dynamics for internal mixtures by the quadrature method of moments, *J. Aerosol Sci.*, *34*, 189–209, 2003.

McNider, R. T., W. B. Norris, A. J. Song, R. L. Clymer, S. Gupta, R. M. Banta, R. J. Zamora, A. B. White, and M. Trainer, Meteorological conditions during the 1995 Southern Oxidation Study Nashville/Middle Tennessee field intensive, *J. Geophys. Res.*, *103*, 22,225–22,243, 1998.

Mebust, M. R., B. K. Eder, F. S. Binkowski, and S. J. Roselle, Models-3 Community Multiscale Air Quality (CMAQ) model aerosol component: 2, Model evaluation, *J. Geophys. Res.*, *108*(D6), 4184, doi:10.1029/2001JD001410, 2003.

Odman, M. T., and C. L. Ingram, Technical report: Multiscale Air Quality Simulation Platform (MAQSIP): Source code documentation and validation, *Rep. ENV-96TR002-v1.0.*, 83 pp., MCNC Environ. Programs, Res. Triangle Park, N. C., 1996.

Odum, J. R., T. P. W. Jungkamp, R. J. Griffin, R. C. Flagan, and J. H. Seinfeld, The atmospheric aerosol-forming potential of whole gasoline vapor, *Science*, *276*, 96–99, 1997.

Ogren, J. A., Asystematic approach to in situ observations of aerosol properties, in *Aerosol Forcing of Climate*, edited by R. J. Charlson and J. Heintzenberg, pp. 215–226, John Wiley, New York, 1995.

Penner, J. E., et al., Comparison of model-and satellite-derived aerosol optical depth and reflectivity, *J. Atmos. Sci.*, *59*, 441–460, 2002.

Rasch, P. J., M. C. Barth, J. T. Kiehl, S. E. Schwartz, and C. M. Benkovitz, A description of the global sulfur cycle and its controlling processes in the National Center for Atmospheric Research Community Climate Model, version 3, *J. Geophys. Res.*, *105*, 1367–1385, 2000.

Roelofs, G. J., et al., Analysis of regional budgets of sulfur species modeled for the COSAM exercise, *Tellus, Ser. B*, *53*, 673–694, 2001.

Russell, L., and J. H. Seinfeld, Size-and composition-resolved externally mixed aerosol model, *Aerosol Sci. Technol.*, *28*, 403–416, 1998.

Seaman, N. L., Meteorological modeling for air-quality assessments, *Atmos. Environ.*, *34*, 2231–2259, 2000.

Schröder, F., B. Kärcher, M. Fiebig, and A. Petzold, Aerosol states in the free troposphere at northern midlatitudes, *J. Geophys. Res.*, *107*(D21), 8126, doi:10.1029/2000JD000194, 2002.

Schwartz, S. E., Mass-transport considerations pertinent to aqueous phase reactions of gases in liquid-water clouds, in *Chemistry of Multiphase Atmospheric Systems*, *NATO ASI Ser.*, vol. G6, edited by W. Jaeschke, pp. 415–471, Springer-Verlag, New York, 1986.

Schwartz, S. E., The whitehouse effect—Shortwave radiative forcing of climate by anthropogenic aerosols: An overview, *J. Aerosol Sci.*, *27*, 359–382, 1996.

Schwartz, S. E., and P. Warneck, Units for use in atmospheric chemistry, *Pure Appl. Chem.*, *67*, 1377–1406, 1995.

Seinfeld, J. H., and S. N. Pandis, *Atmospheric Chemistry and Physics of Air Pollution*, 1326 pp., John Wiley, New York, 1998.

Shaw, R. W., Jr., and R. J. Paur, Measurements of sulfur in gases and particles during sixteen months in the Ohio river valley, *Atmos. Environ.*, *17*, 1431–1438, 1983.

Sherman, D. E., S. Kreidenweis, and T. McKee, The influence of synoptic and local meteorological conditions on ambient particle concentrations during the southeastern aerosol and visibility study (SEAVS), Coop. Inst. for Res. in the Atmos., Colo. State Univ. and Latimer and Assoc., Boulder, Colo., 1997.

Sisler, J. F., and W. C. Malm, Interpretation of trends of $PM_{2.5}$ and reconstructed visibility from the IMPROVE network, *J. Air Waste Manage. Assoc.*, *50*, 775–789, 2000.

Tang, I. N., and H. R. Munkelwitz, Water activities, densities, and refractive indices of aqueous sulfates and sodium nitrate droplets of atmospheric importance, *J. Geophys. Res.*, *99*, 18,801–18,808, 1994.

Von Salzen, K., H. G. Leighton, P. A. Ariya, L. A. Barrie, S. L. Gong, J. P. Blanchet, L. Spacek, U. Lohmann, and L. I. Kleinman, Sensitivity of sulfate aerosol size distribution and CCN concentrations over North America to SO_x emissions and H_2O_2 concentrations, *J. Geophys. Res.*, *105*, 9741–9765, 2000.

Walcek, C. J., and G. R. Taylor, A theoretical method for computing vertical distributions of acidity and sulfate production within cumulus clouds, *J. Atmos. Sci.*, *43*, 339–355, 1986.

Whitby, K., The physical characteristics of sulfur aerosols, *Atmos. Environ.*, *12*, 125–159, 1978.

Whitby, E., and P. H. McMurry, Modal aerosol dynamics modeling, *Aerosol Sci. Technol.*, *27*, 673–688, 1997.

Wilson, J., C. Cuvelier, and R. Raes, A modeling study of global mixed aerosol fields, *J. Geophys. Res.*, *106*, 34,081–34,108, 2001.

Woo, K. S., D. R. Chen, D. Y. H. Pui, and P. H. McMurry, Measurement of Atlanta aerosol size distributions: Observations of ultrafine particle events, *Aerosol Sci. Technol.*, *34*, 75–87, 2001.

Wright, D. L., Retrieval of optical properties of atmospheric aerosols from moments of the particle size distribution, *J. Aerosol Sci.*, *31*, 1–18, 2000.

Wright, D. L., R. McGraw, C. M. Benkovitz, and S. E. Schwartz, Six-moment representation of multiple aerosol populations in a sub-hemispheric chemical transformation model, *Geophys. Res. Lett.*, *27*, 967–970, 2000.

Wright, D. L., P. S. Kasibhatla, R. McGraw, and S. E. Schwartz, Description and evaluation of a six-moment aerosol microphysical module for use in atmospheric chemical transport models, *J. Geophys. Res.*, *106*, 20,275–20,291, 2001.

Wright, D. L., S. C. Yu, P. S. Kasibhatla, R. McGraw, S. E. Schwartz, V. K. Saxena, and G. K. Yue, Retrieval of aerosol properties from moments of the particle size distribution for kernels involving the step function: Cloud droplet activation, *J. Aerosol Sci.*, *33*, 319–337, 2002.

Yu, S. C., V. K. Saxena, B. N. Wenny, J. J. DeLuisi, G. K. Yue, and I. V. Petropavlovskikh, A study of the aerosol radiative properties needed to compute direct aerosol forcing in the southeastern United States, *J. Geophys. Res.*, *105*, 24,739–24,749, 2000.

Yu, S. C., C. S. Zender, and V. K. Saxena, Direct radiative forcing and atmospheric absorption by boundary layer aerosols in the southeastern United States: Model estimates on the basis of new observations, *Atmos. Environ.*, *35*, 3967–3977, 2001.

Yue, G. K., J. Lu, V. A. Mohnen, P.-H. Wang, V. K. Saxena, and J. Anderson, Retrieving aerosol optical properties from moments of the particle size distribution, *Geophys. Res. Lett.*, *24*, 651–654, 1997.

A. Deng, Department of Meteorology, Pennsylvania State University, University Park, PA 16802, USA.

P. S. Kasibhatla and D. L. Wright, Nicholas School of the Environmental and Earth Sciences, Duke University, Durham, NC 27708, USA.

R. McGraw and S. E. Schwartz, Atmospheric Sciences Division, Brookhaven National Laboratory, Upton, NY 11973, USA.

S. Yu, U.S. Environmental Protection Agency, National Exposure Research Laboratory, Atmospheric Science Modeling Division (E243-01), Research Triangle Park, NC 27711, USA. (yu.shaocai@epa.gov)

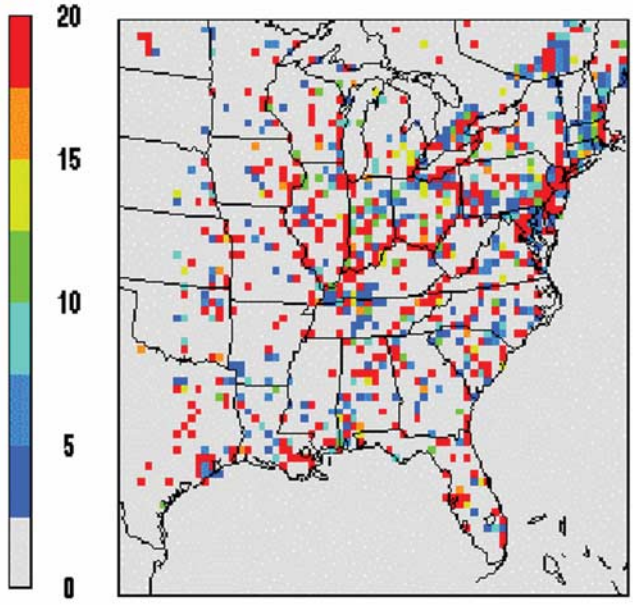

Figure 1. The MAQSIP model domain and distribution of sulfur ($SO_2 + SO_4^{2-}$) emission over the eastern United States in summer, including both surface and elevated sources (see text). Unit is g m^{-2} yr^{-1}.

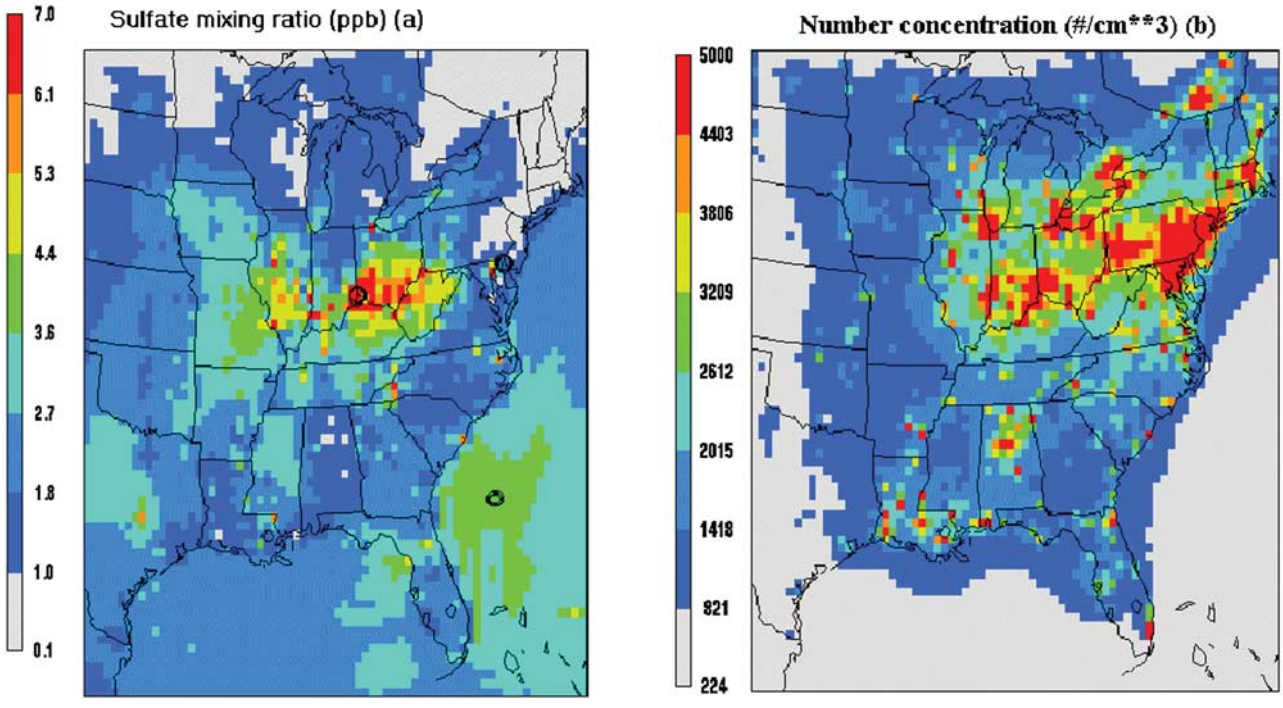

Figure 12. The 40-day average values of the horizontal distributions of (a) mean sulfate mixing ratios (ppb) and (b) number (μ_0, cm^{-3}) concentrations at the lowest model layer. Circles at Ohio River valley, New Jersey, and the Atlantic Ocean east of Georgia in Figure 12a denote the locations selected for budget analysis (see the explanation in text). The middle cells of the surrounding nine cells (3 × 3) for each area are cell (60,50) (latitude: 39.41°N, longitude: −76.13°W), cell (40,46) (latitude: 38.87°N, longitude: −84.86°W) and cell (60,22) (latitude: 30.31°N, longitude: −77.94°W) for New Jersey area, Ohio River valley, and Atlantic Ocean, respectively.